HIGH ENERGY IMPACT ROCK BREAKAGE RESEARCH PROGRAM ANNUAL REPORT MARCH 1972 REPORT TM-7204

Prepared by
Ingersoll-Rand Research, Inc.
P. O. Box 301
Princeton, N.J. 08540
Phone (609) 921-9103

Joel W. Hollenberg
Principal Investigator

Lee W. Yaros
Development Engineer

Mukund D. Gangal
Solid Mechanics Analyst

Sponsored by
Advanced Research Projects Agency
ARPA Order No. 1579, Amend. 2
Program Code 1F10

Monitored by
Bureau of Mines
Contract No. H0210045
Amount of Contract $59,944.00
Effective Date: 23 March 1971
Contract Expiration 23 March 1972

85

DISCLAIMER NOTICE

THIS DOCUMENT IS THE BEST QUALITY AVAILABLE.

COPY FURNISHED CONTAINED A SIGNIFICANT NUMBER OF PAGES WHICH DO NOT REPRODUCE LEGIBLY.

The views and conclusions contained in this document are those of the authors and should not be interpreted as necessarily representing the official policies either expressed or implied of the Advanced Research Projects Agency or the United States Government.

Ingersoll-Rand Research, Inc.
P. O. Box 501
Princeton, N.J. 08540

HIGH ENERGY IMPACT ROCK BREAKAGE RESEARCH PROGRAM

Annual Report - October 1971 through March 1972

Joel W. Hollenberg
Lee W. Yaros
Maynard D. Gargiul

16 May 1972 | 92 | 13

H0210045

TM-7201

ARPA Order No. 1579
Amendment 2
Program Code 1F10

Unlimited

Advanced Research Projects Agency
Washington, D.C. 20301

The purpose of this program is to study the effect of factors such as tool shape, blow energy, single and multiple location impacts and spacing on the fragmentation of hard rock. The major activities within the project include:

A. Theoretical Analysis and Parameter Study
B. Fracture Tests on Barre Granite
C. Field Tests in Various Formations

Annual results are reported here for each of these activity areas. The goal of the program is to obtain a better understanding of mechanical rock breakage in order to provide for a faster, more economical method of underground excavation in hard rock formations to be eventually developed.

Details of illustrations in this document may be better studied on microfiche

DD FORM 1 NOV 65 1473

Unclassified
Security Classification

I

KEY WORDS						
Breakage, Rock						
Impact						
Fragmentation						
Hammer, Hydraulic						
Fracture						

TABLE OF CONTENTS

III

LIST OF FIGURES

III

LIST OF PLATES

TECHNICAL REPORT SUMMARY

The purpose of this project is to study, by means of theoretical analysis, laboratory experimentation, and field testing, the effect of blow energy, tool shape, single- and multiple-location impacts and spacing on the fragmentation of rock, in-situ and for blocks. The overall primary goal is to obtain a better understanding of mechanical rock breakage which can provide a faster, more economical method of excavation, tunneling, or large-hole drilling in hard underground rock formations, and to examine the potential special advantages with respect to noise and dust generation as well as remaining formation stability that this method may enjoy.

During the first meeting on the High Energy Impact Excavation Project, the utilization of the high-energy impact tool was visualized as occurring in a two-step process. First, one must produce large cracks in the rock mass and then, produce secondary fractures fragmenting the rock into pieces. During the past year both of these areas were studied, analytically and experimentally. Excellent quantitative information was obtained which will provide basic information for all future work on the project.

The major conclusions reached are summarized below.

1. A qualitative understanding has been reached regarding the subsurface fracture produced by impact in rock.

2. Reproducible and controlled cracking is obtained with a wedge-shaped indentor.

3. A quantitative relationship has been established between blow energy and crack length for a wedge-shaped indentor.

4. Qualitative as well as quantitative understanding has been reached in the case of edge fracture.

5. A critical level of blow energy exists at which a piece of rock breaks out from the edge.

6. The volume of rock broken out in edge fracture is principally a function of edge distance and tool shape.

7. Hatenyi's analysis* seems to explain the nature of the edge fracture. More rock testing will be needed to prove the variation of critical blow energy as a function of rock tensile strength and tool wedge angle.

8. Low specific energies demonstrated during the edge fracture tests show promise for a tunneling system application.

---

* This will be explained in detail in Section II-B of this report.

I. OBJECTIVE AND SCOPE

The objective of this research program is to study the effect of factors such as tool shape, blow energy, single- and multiple-location impacts and spacing on the fragmentation of hard rock samples. The primary goal of this work will be to obtain a better quantitative understanding of mechanical rock breakage which can provide a faster, more economical method of excavation, tunneling, or drilling in hard underground rock formations.

The work is divided into three main activity areas; these are as follows:

1. Analytical and experimental study of subsurface cracking.
2. Analytical and experimental study of edge fracture (or secondary breakage).
3. Field tests in various formations.

Each of these areas will be reported upon in the following sections of this report. The purpose of each of these activity areas is as follows.

1. Analytical and Experimental Study of Subsurface Cracking.

This work is aimed at providing a guide for the application of high-blow energy impact tools in rock excavation. Through the mathematical modeling of the rock impact process, utilizing existing and modified theories, relationships were sought between impact tool parameters such as blow energy, tool shape, etc., and rock properties, which can be used in designing and operating impact excavation equipment for tunneling into a solid face of hard competent rock. Of principal concern is the relationship between tool and rock properties in terms of the size and direction of subsurface cracks which can be produced.

2. Analytical and Experimental Study of Edge Fracture (or Secondary Breakage).

This work is aimed at providing a quantitative description of this process which is visualized as breaking to an edge in the rock which either pre-exists or is created in a massive formation by fractures produced as a result of a sufficiently high-blow energy primary impact (see above). Through

analytical investigations and laboratory testing utilizing our drop tower facility, relationships were sought among blow energy, tool shape, edge distance, and material removed (specific energy fracture) for Barre granite.

3. Field Tests in Various Formations.

This work was aimed at providing preliminary experience in in-situ rock removal for hard, massive formations. Through these field tests, an appreciation of the actual problems which would be encountered using the impact rock removal process during tunneling by means of this method was gained. To date, three such trials have been carried out, one in a diabase formation near Belle Mead, N.J. and two in a granite gneiss formation near Mt. Hope, N.J. The field testing at Belle Mead was reported upon in the Semiannual Report. Section II-C of this report covers the testing at the Mt. Hope quarry.

II. MAJOR ACCOMPLISHMENTS

A. Subsurface Cracking

1. Introduction

Cratering phenomena related to indentation of rocks, have been observed experimentally and studied analytically by several investigators including Fairhurst and Lacabanne[1*], Reichmuth[2], Paul and Sikarski[3], and Sikarski and Miller[4]. They observed that when wedge-shaped and button-shaped tools impact rock, the rock ahead of the tool is crushed, forming a "crater," and then, depending upon the impact energy, chips of rocks may break out at the surface. In addition, they invaribly observed that tensile cracks of rather large size compared to crater size were present at the bottom of the crater. However, their observations on subsurface cracking were essentially qualitative. From the start of the program on High Energy Impact Tunneling, it was recognized that this subsurface cracking may play an important role in this overall rock fragmentation process, and hence we set out to determine the quantitative relationships involved in subsurface cracking.

Earlier workers showed that for impact velocities encountered in drilling, the dynamic effects may be ignored. Therefore, they modeled the wedge indentation process by a line load on an elastic half-space and were puzzled by finding that the stresses they calculated within the solid were everywhere compressive while the cracks indicated tensile stresses. At this point, Paul and Gangal[5] used a more realistic model by assuming a quasi-hydrostatic loading on the crater, and showed that around the crater, one component of the stresses was indeed tensile with large enough magnitude to allow tensile cracking.

Recent work of Aquino[6] at Bell Labs appears to be the first study of the quantitative aspects of the subsurface cracking phenomena of spherical indentors. His work was reviewed in the semiannual[7] report on this project. From analytical expressions, he introduced an important concept, namely the linear relationship between contact radius of the indentor and the crack size. This observation can be used with a modified interpretation to determine crack size in rock, as will be explained later.

---

* Superscript Numbers indicate References in Section V.

In what follows, we will report first upon a semi-empirical model used to study the cracking phenomena, then we will present the results of our experiments, and finally we will state the conclusions.

2. Semi-Empirical Model

In this subsection, we will consider a semi-empirical model for an indentor impacting a flat surface of rock. At the beginning of impact the indentor and the rock surface are deformed elastically according to the Hertz theory until the load exceeds the crushing strength of the rock. Above this initial crushing point, the tool creates a zone of highly-pulverized rock which we call a "crater." The powdered rock material compacted between the crater surface and the tool is probably under a "quasi-hydrostatic" state of compression. Depending upon the rock properties one or more surface chips may also be formed during the process of cratering. However, this chipping (which is important in drilling) need not concern us here. In the following discussion we will be interested in investigating the effects of the quasi-hydrostatic loading on the crater.

Figure 1 shows schematically the tool indentation process. For a spherical-tipped indentor, the crater will be idealized simply by a hemispherical cavity under uniform pressure, bounded by a semi-infinite solid (rock) as also shown in Fig. 1. Alternately, for a wedge-shaped tool the crater will be idealized by a pressurized hemicylindrical crater. Although the idealized problems look simple no analytical solutions are available in the literature. Therefore, it was decided to use the finite element method to solve the idealized crater problem. The solution for the hemispherical case was obtained using a computer programs developed for the stress stress analysis of axisymmetric solids. Solution for the hemicylindrical crater is taken from Paul and Gangal[5]. Since all geometric dimensions can be scaled in terms of the crater radius, R, unit crater radius was used in the computation. To simulate the semi-infinite nature of the rock, the outer boundary was chosen to have a radius which was of the order of forty times larger than the crater radius and a stress field consistant with the theoretical point load and line load soultions (for details see Ref. 5).

The crater pressure, p, is very difficult to measure. It is a function of overall tool shape, energy, and rock type. Let us non-dimensionalize the stresses with respect to the pressure, p. For simplicity a unit normalized pressure was used in the finite element computation. In reality, the pressure will always be greater than σ_c, the compressive strength of the rock

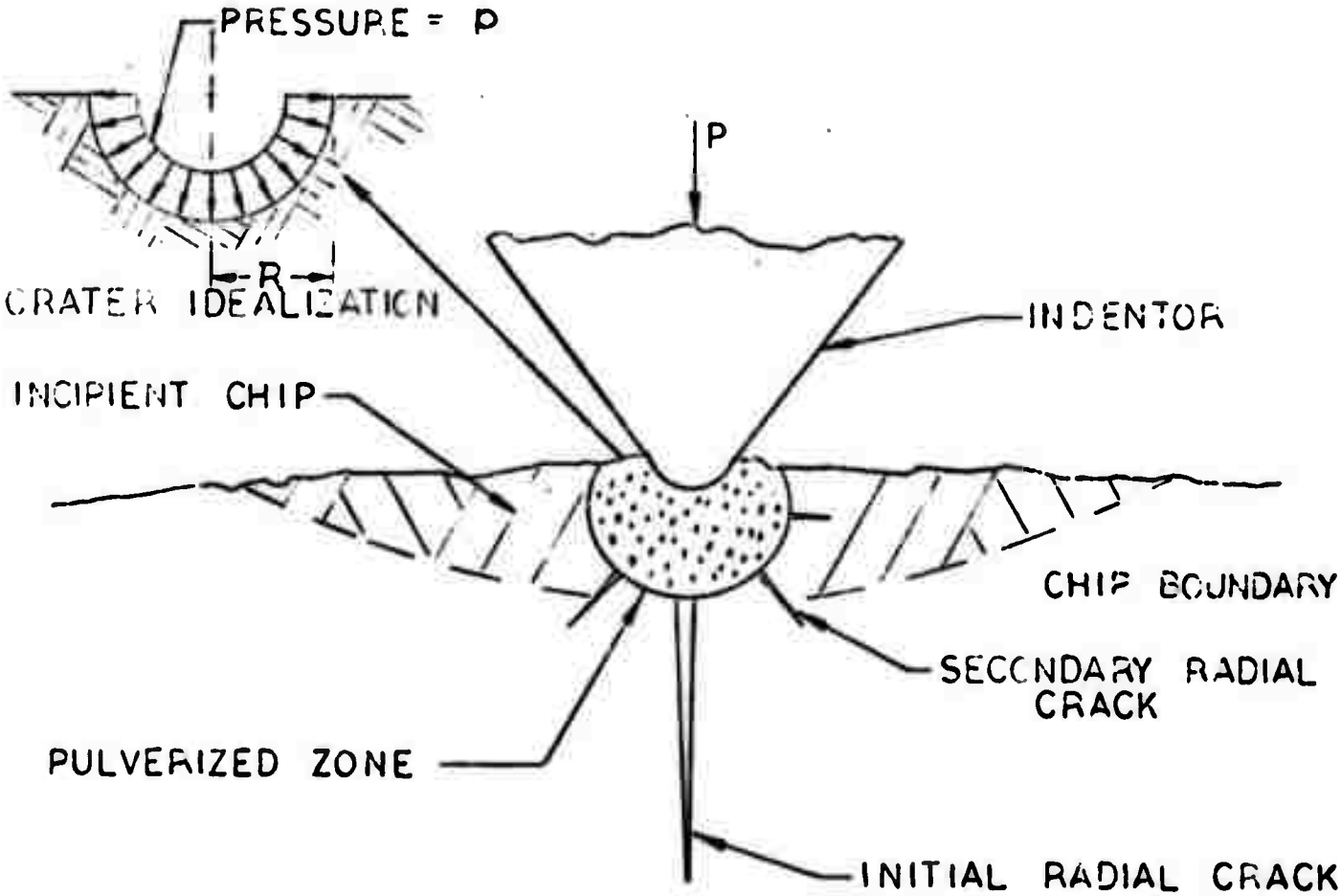

INITIAL CRACK FORMATION

FIGURE 1

Figure 2 shows the distribution of the tangential stress, σ_θ, plotted as a function of radius. The figure also shows a stress contour representation of σ_θ. The tensile strength of the rock, σ_t, is usually small compared to its compressive strength. The tensile stress at the bottom of the crater on the other hand is of the order of the crater pressure which is larger than the compressive strength of the rock. Thus one would expect a crack to form and grow along the center line of the crater. In addition to this central crack several smaller cracks can also be formed as shown in Ref. 5.

Figure 3 shows the distribution of the hoop stress for the hemispherical crater. At the bottom of the crater, the hoop stress approaches to a value of roughly half the crater pressure. Thus one would again expect cracking to occur. Note, however, that in this case the tensile hoop stress field is axi-symmetric and therefore does not have a preferred direction to propagate a crack. Thus one should expect in this case that the formation of a single crack or multiple cracks, the directions etc. to be determined by rock anisotropy, inhomogeniety, and the pressure of pre-existing microcracks rather than the stress field. Once initiated, these cracks may grow in the tensile stress region to a length, say, ℓ, which can be several times larger than crater radius, R. Thus,

$$\ell = \alpha R \qquad (1)$$

where α is a constant for a given material and tool shape to be evaluated experimentally.

Aquino[6] followed a somewhat different course. He used the Hertz theory to determine an equivalent of the pressure, p. Then he used Love's analytical solution to obtain the tensile stress (hoop) distribution. At that point he departed from the above method and used an approximate Griffith's approach to determine the crack size as a function of Hertz contact radius. He then derived a relationship between "crack radius" and the equivalent of crater radius, R, which is similar to the relationship (1) above, and evaluated the constant experimentally.

From a more practical viewpoint, in a given rock the most important relationship is between crack length and blow energy. In the literature on craters, various investigators* report widely different relationships between crater depth (which equals our crater radius, R) and the blow energy. However, one may write a general expression of the form:

---

* see references 1, 2, 3.

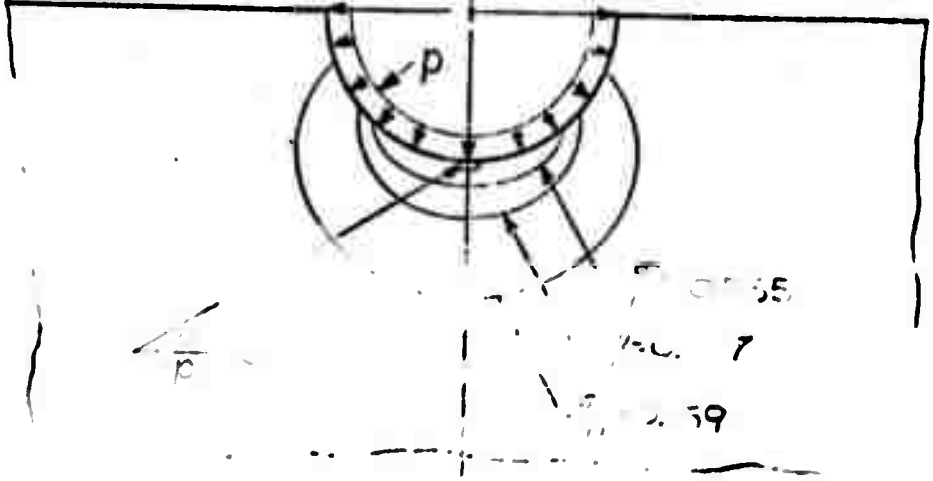

CONTOUR LINES OF EQUAL TENSILE STRESS

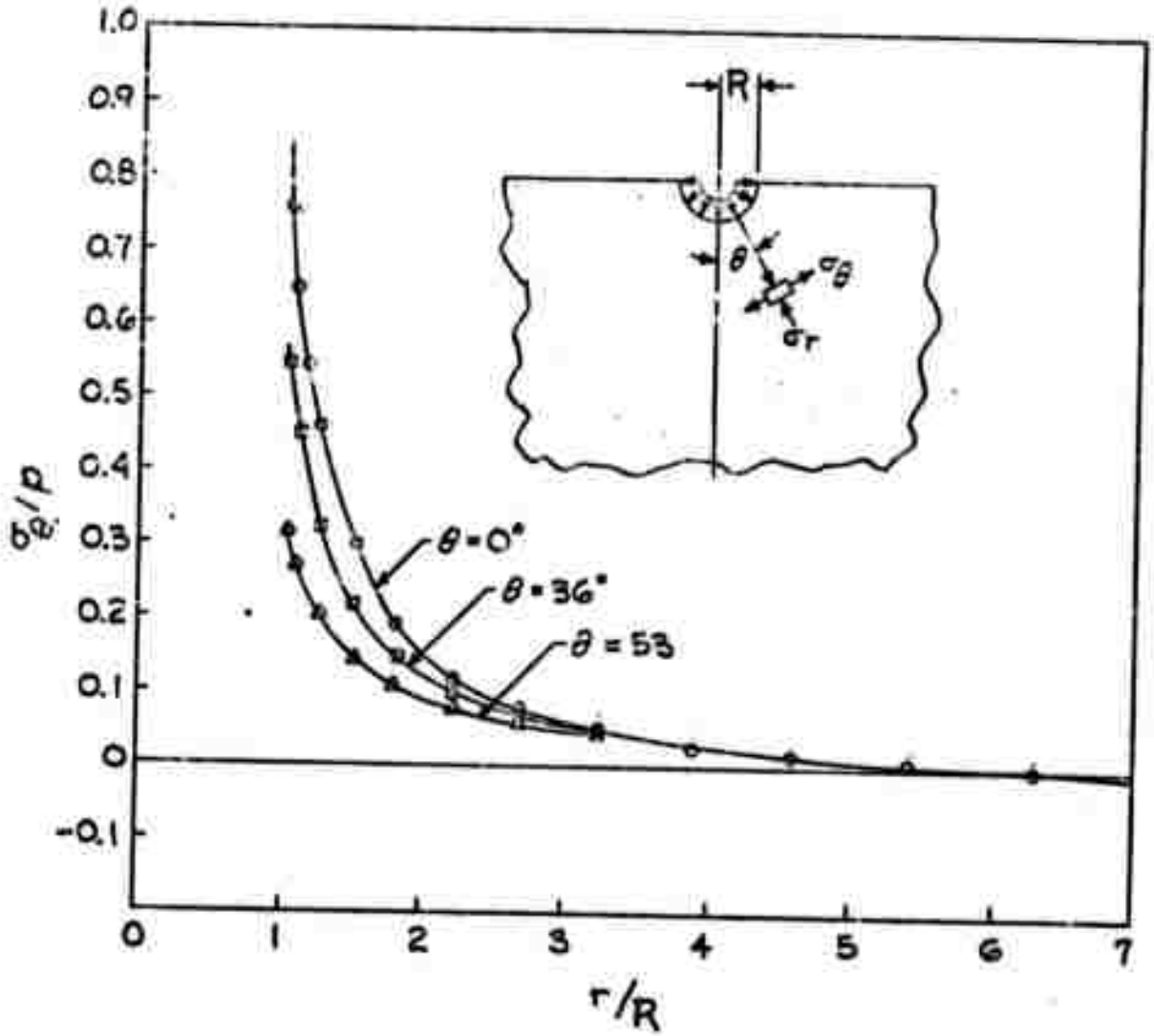

DECAY OF TENSILE STRESS WITH RADIUS
FOR A SEMI-CYLINDRICAL CRATER

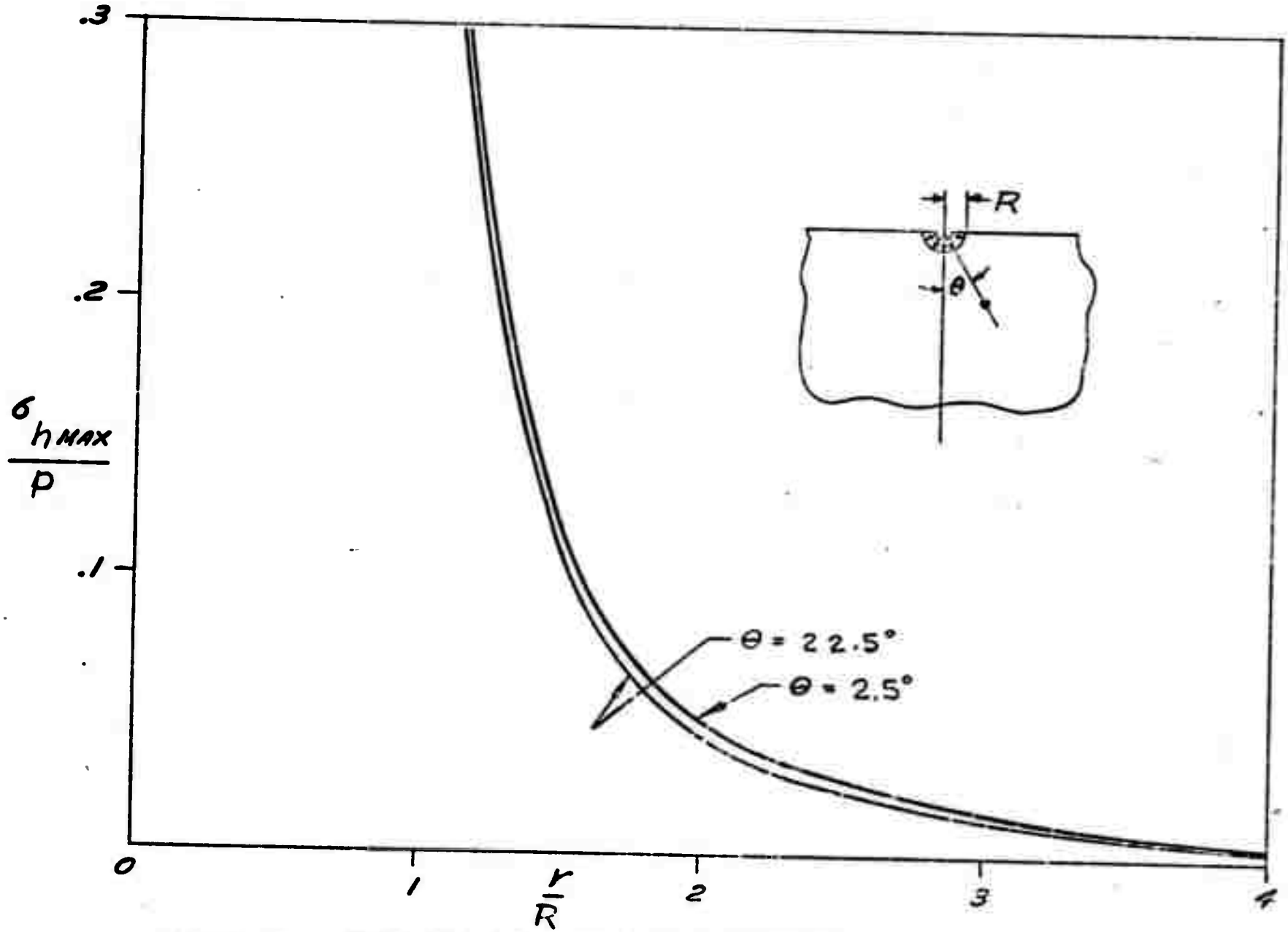

FIGURE 3: DECAY OF TENSILE STRESS WITH RADIUS FOR HEMISPHERICAL CRATER

$$R \alpha E^n \qquad (2)$$

where E = blow energy for the spherical indentor and blow energy per unit length for the wedge-shaped indentor, and n = an emperical constant.

Thus, the crack length is also related to E as shown below

$$\ell = K_1 E^n$$

The constant of proportionality and the exponent, n, are determined experimentally.

3. Experimental Verification

It was recognized quite early in the program that quantitative measurements on subsurface cracking to establish all parametric relationships would be very costly. A limited series of experiments were therefore planned to study the most important parameters, namely the input energy and basic tool shape, i.e., the spherical tool vs. the wedge-shaped tool.

The object of the experimental program was twofold: first, to see if reproducible subsurface cracking could be produced in the rock, and then, if successful, to obtain a quantitative relationship between the crack length and the tool-rock parameters. It was decided that the first objective could be attained by static indentation tests while the second objective required impact tests. These are described in turn below.

(a) Static Tests

For the purpose of the limited experimental program, eight 9 inch Barre granite cubes were obtained. Two basic tool shapes were chosen, a 7/16 inch sphere and a 1 inch by 3/8 inch, 120° wedge. In an exploratory phase of the work, a single block was indented on faces marked B, B', C, and C' in Fig. 4 with the spherical-tipped tool. Then a dye penetrant was applied to the crater and after waiting for about half an hour, the block was split open to trace subsurface dye penetration into the crack. It was found that the dye diffused into a large hemispherical zone under the crater. This wiped out any distinction between cracked and solid rock. This technique was therefore proven to be inapplicable.

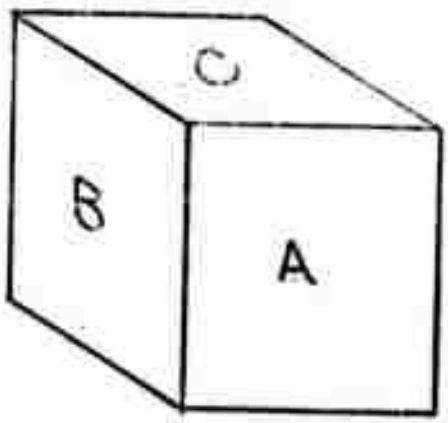

FIG. 4 : ROCK FACE DESIGNATION.

NOTE: A', B' AND C' ARE FACES OPPOSITE TO FACES A, B AND C RESPECTIVELY.

Next, an X-ray radiography technique was used. Here the rocks were first radiographed to show the initial state. Then one of the rocks was indented and x-rayed again and compared with the initial radiograph. It was found that cracks could not be detected with this technique either.

Finally, a rock indented with the 7/16 inch spherical tipped tool was cut with a diamond saw through the center of the craters, parallel to face A It was found that the large cracks starting at the crater were visible to the eye. To increase the contrast a special dye penetrant, P-135 made by Trace Tech, was used. This dye penetrant is sensitive to ultraviolet light. After dye penetration, each crack was photographed using ultraviolet light. Plates 1 through 4 show the photographs of the four craters and the cracks produced with the 7/16 inch spherical indentor.

Plates 1 through 4 yielded the following observations. Only in one case (Plate 1) was a central crack observed. In two cases (Plates 2 and 3) cracks smaller in size and propagating at different angles than that observed in Plate 1 were detected. Finally there were cases such as shown in Plate 4 where no single major crack was observed. It was therefore concluded that with the spherical tip, the direction and size of the major crack could not be controlled. Similar experiments with wedges showed rather good predictability, and therefore, all impact tests using spherical tips were abandoned.

(b) Impact Tests

The objective of these tests was to establish the important relationship between blow energy and the crack length for a given wedge-shaped tool. A 1 inch long, 3/8 inch wide, tungsten-carbide wedge (120° inclined angle) shaped bit was cemented at the tip of an impacting moil. Our drop tower facility* was used in the experiments. The 9 inch Barre granite cubes were secured at the bottom, and the moil was dropped on them from predetermined heights. Indentations were made on faces B, B', C, and C'. The blocks were then cut in half with a diamond saw in such a way that the cut passed through the centers of each crater. Once again, Trace Tech P-135

* The drop tower facility and its operation has been described in the Semi-annual Report. Further description of this facility is given later in this report.

PLATE 1: Subsurface Crack #1

Tungsten Carbide
7/16" Spherical Indentor
Static Indentation

PLATE 2: Subsurface Crack #2

Tungsten Carbide
7/16" Spherical Indentor

PLATE 3: Subsurface Crack #3

Tungsten Carbide
7/16" Spherical Indentor
Static Indentation

PLATE 4: Subsurface Crack #4

Tungsten Carbide
7/16" Spherical Indentor
Static Indentation

PLATE 5: Subsurface Crack #5

Tungsten Carbide
1" x 3/8", 120° Wedge Shaped Indentor
Blow Energy = 55 ft-lbs

PLATE 6: Subsurface Crack #6

Tungsten Carbide
1" x 3/8", 120° Wedge Shaped Indentor
Blow Energy = 55 ft-lbs

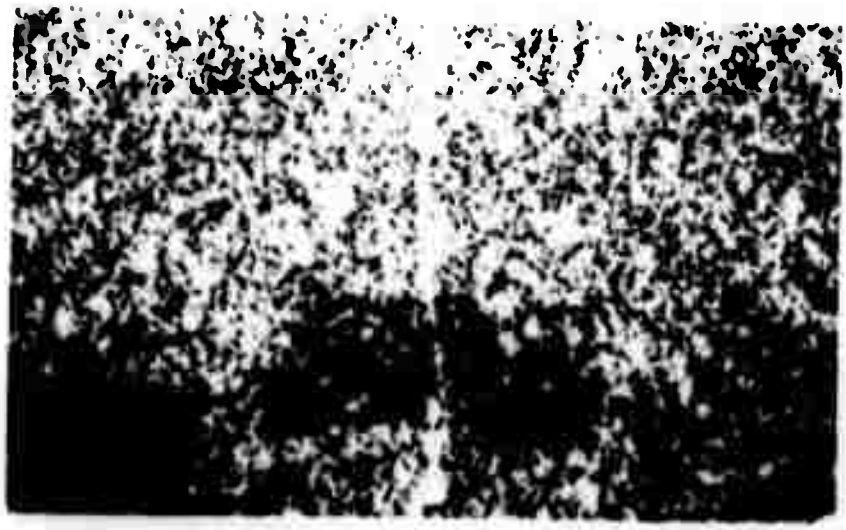

PLATE 7: Subsurface Crack #7

Tungsten Carbide
1" x 3/8", 120° Wedge Shaped Indentor
Blow Energy = 55 ft-lbs

PLATE 8: Subsurface Crack #8

Tungsten Carbide
1" x 3/8", 120° Wedge Shaped Indentor

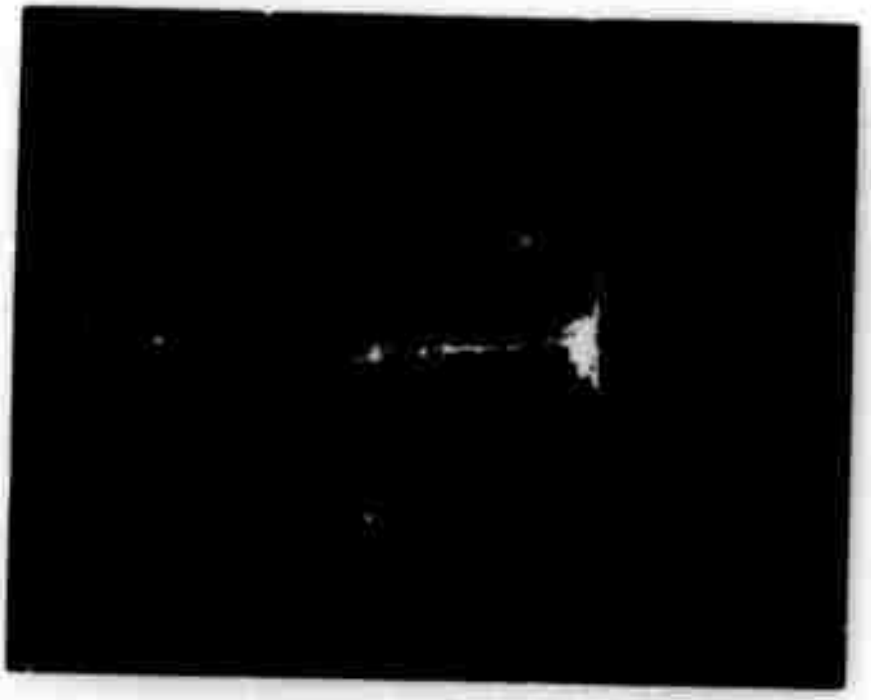

PLATE 9: Subsurface Crack #9

Tungsten Carbide
1" x 3/8", 120° Wedge Shaped Indentor
Blow Energy - 110 ft-lbs

PLATE 10: Subsurface Crack #10

Tungsten Carbide
1" x 3/8", 120° Wedge Shaped Indentor

dye was used to detect cracks. Plates 5 through 10 show the results. Each of these plates shows an indentation corresponding to a blow energy marked under the plate. In every case a major crack was produced roughly following the centerline of the crater. Crack lengths were measured on the actual block. In other experiments (at energies beyond 150 ft lb) crack photographs could not be obtained because the blocks split open after two or more blows. In these cases crack length was determined by visual observation.

(c) Observations

1. The techniques described above yield satisfactory measurement of depth of crack penetration. Cracks observed are several times larger than the crater depth.

2. At blow energy levels of the order of 330 ft lb, the blocks split open indicating crack lengths of the order of 4-1/2 in. (half the block size).

3. Figure 5 shows the plot of blow energy vs. crack length for the wedge plotted on a log-log scale. This gives the following expression:

$$\ell = 0.093\ E^{0.67} \qquad (4)$$

for the particular wedge and granite block combination used in the experiment.

At this stage, the information generated here is sufficient to allow order of magnitude estimates needed in design studies of impact excavators. However, more reliable values of K and n should be obtained by conducting additional tests in the future, especially for different rocks.

4. Concluding Remarks on Subsurface Cracking

The work described in this section of the report shows the following:

(a) It confirms the existence of subsurface cracks which are several times larger than the main crater dimensions.

(b) Spherical tipped tools do not produce repeatable results in that the crack direction and size are quite variable and uncontrolled.

(c) Wedge-shaped tools produce consistent cracks. The major crack starts at the bottom of the wedge and progresses approximately in the plane of symmetry of the wedge.

(d) The limited set of experiments indicates a linear relationship between crack length and blow energy as (4) above.

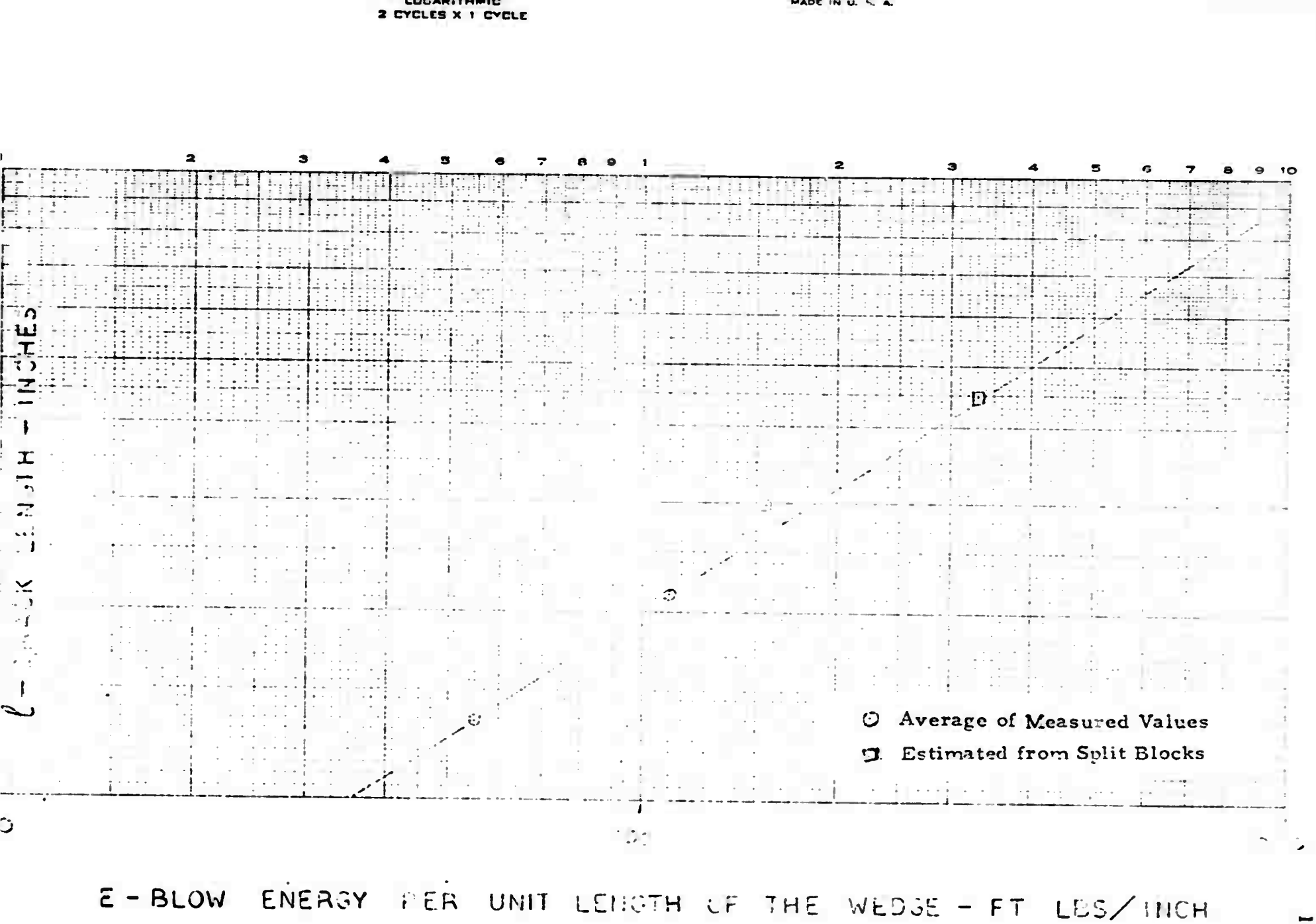

FIGURE 5
VARIATION OF CRACK LENGTH WITH BLOW ENERGY

To illustrate the meaning of these results, if a tool with 10,000 ft lb of blow energy and an 8 inch long wedge were to be used, cracks as long as 10-1/2 inch in Barre granite could be produced. This is a reasonable size for use in impact tunneling devices. A bigger tool, of course, can produce a larger crack and, therefore, is more desirable. Alternatively, reducing the length of the wedge will produce deeper, but less wide, cracks. One must also keep in mind the possible tool wear which will limit the energy per unit leng of the wedge. In the actual impactor and tool design work to be carried out next year one of the tasks will be to balance these two factors.

B. Edge Fracture

1. Introduction

In this section we will examine one of the important modes of secondary fracture; i.e., the edge fracture mode (see Figures 6 and 7).

The problem of rock fracture to an edge is similar to the indexing problem in conventional percussive drill systems. The latter has been studied by numerous investigators, including Simon, Cooper, and Stoneman[8], Hartman[9], and Garner[10]. In particular, Garner used the photoelastic model technique and observed the tensile stress field which causes the edge fracture. Evans[11] studied a more closely related problem. He analyzed the two-dimensional equivalent of the edge fracture problem, namely the action of a wedge producing breakage into a buttock of coal. An equilibrium approach such as used by Evans for coal (Fig. 6) was not used here because hard rocks such as granite tend to behave in a brittle manner. Once a crack is started it can propagate rapidly in a suitable tensile stress field and therefore the stress along the parting surface need not reach the tensile limit all at once.

The analysis in this report will be based upon some recent work done by Hatenyi[12, 13]. In the following sections, the basic aspects of the analysis will be explained first, and then the results will be correlated with experimental data.

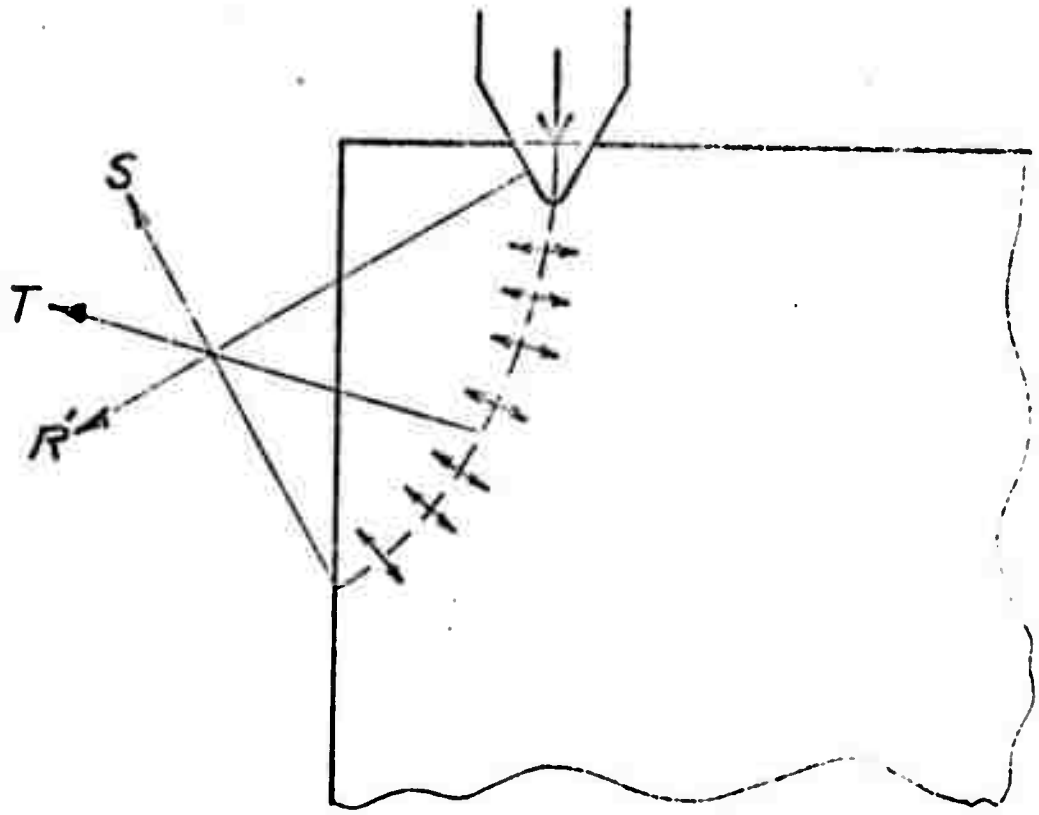

R'- Wedge force
T - Equilibrium tensile force
S - Tip reaction

Figure 6: Evans' Equilibrium Approach for Cutting Coal

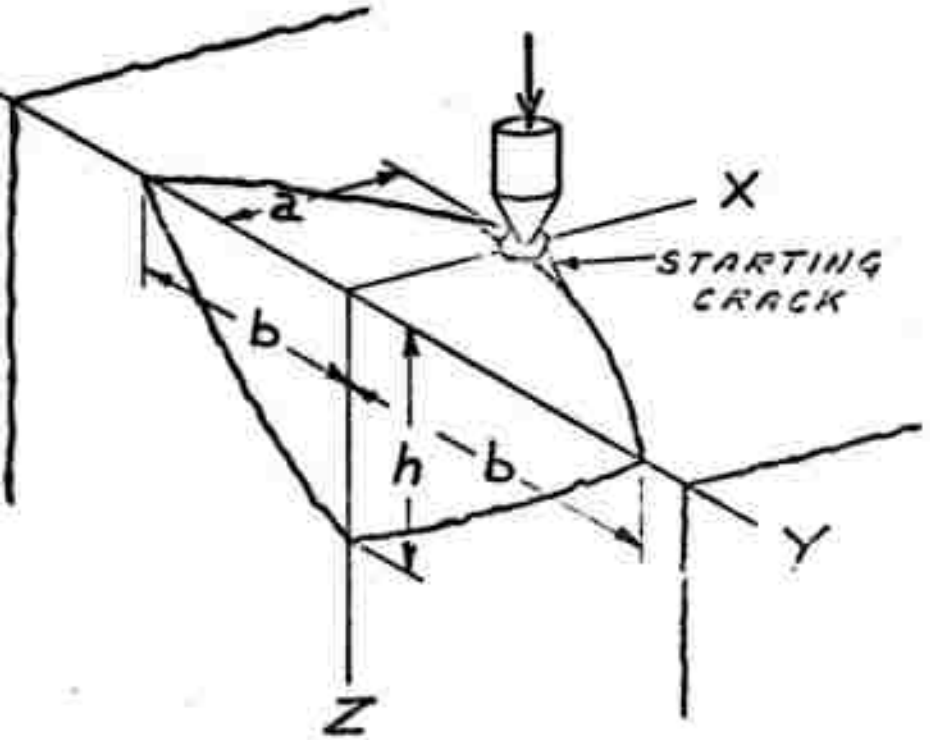

Figure 7-a: Action of the Moil in Edge Fracture

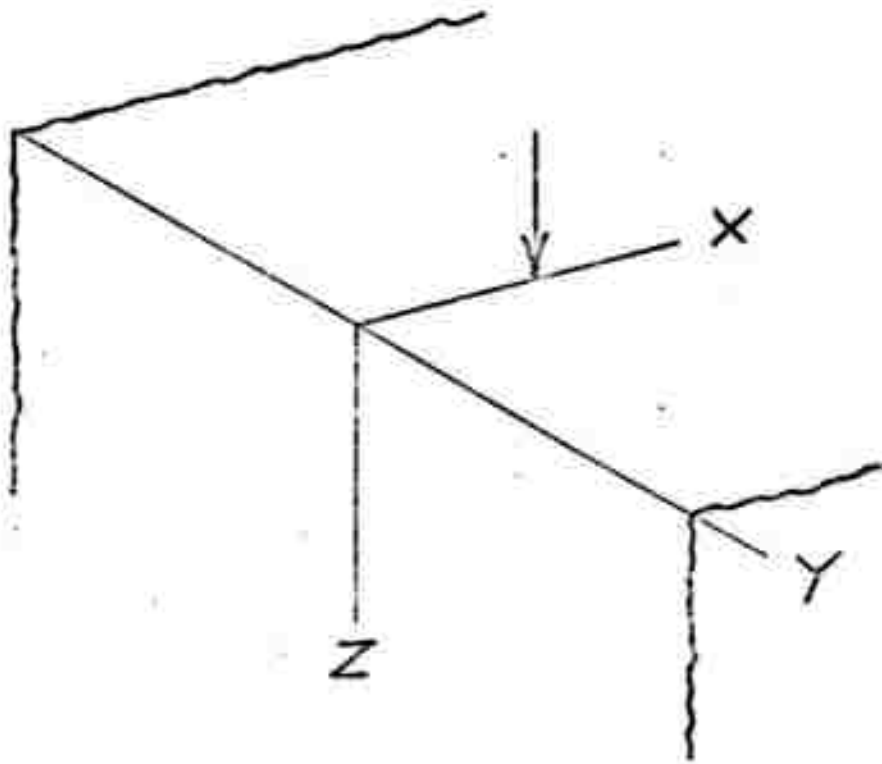

Figure 7-b: Quarter-space Idealization

2. Edge Fracture for Pointed Indentors

In view of the previous considerations, the stress field produced by indentors is investigated with two specific questions in mind: (a) Does the stress field lead to crack initiation? and (b) can one get some clues as to the general shape of the final fracture? In what follows it will be shown that Hatenyi's solution to the elastic quarter space sheds light on the two questions for a pointed indentor and his quarter plane solution gives similar information for a wedge shaped tool.

An impact by a pointed tool in the neighborhood of a large preliminary crack can be idealized for the purpose of mathematical analysis by what is called a quarter-space problem, as illustrated in Figure 7. Recently, Hatenyi presented the theoretical solution to the problem of a point load applied at a distance, a, from the edge of such a quarter-space. Here, Hatenyi's[12] solution will be used to study the edge fracture problem.

Boussinesq solved the problem of a point load acting on an elastic half-space. Using Boussinesq's solution and a clever imaging technique, Hatenyi derived the solution to the quarter-space problem in the form of a series of integral equations. These integral equations are too complicated to be evaluated in the form of analytical expressions. He, therefore, obtained the solutions numerically for four different values of the Poisson's ratio, ν. Here we need not go into the mathematical details of Hatenyi's work, but rather look directly at the results.

There is a mathematical singularity at the point of action of the force ($x = a$, $y = z = 0$). However, the scheme of successive approximation used by Hatenyi in evaluating the series of integral equations is based upon the distributed load solution due to Love. This removes the singularity and

produces smooth stress distributions. The action of the moil in reality creates a small crater with some state of quasi-hydrostatic pressure loading. Thus the Love approximation used by Hatenyi probably represents the real loading better than the mathematically singular point loading. In our particular application, we are interested in σ_x (Fig. 8). When the maximum value of σ_x reaches the tensile strength of the rock, a crack can be initiated as depicted in Fig. 7-a. This crack will then be able to grow and reach the free surface. The stress distribution shown in Fig. 8 is for a solid with Poisson's ratio, $\nu = 1/2$. As ν changes, the stress distributions also change. Table B-1 shows the stress fields for various values of Poissons ratio. One can see from the table that σ_x along the x axis assumes rather large value near the point of action of the tool. For a truly point loading σ_x would become infinitely large under the tool. However, in Hatenyi's solution (in which the load is smeared out), the maximum of σ_x occurs at $x \approx 1.07a$ for Poissons ratios less than 1/3. Table B-2 gives the peak values of σ_x and the location at which they occur.

In this particular case, it turns out that the stresses are linear functions of the Poisson's ratio. Figure 9 shows the plot of non-dimensional maximum σ_x plotted against the Poisson's ratio, ν. Thus, one can say that when the stress maximum, σ_x, which occurs at $x \approx 1.07a$, exceeds the tensile strength of the rock a crack can initiate as shown in Fig. 7. From Figure 9 we can write that

$$\sigma_{x_{max}} = k \frac{P}{a^2} = [7.2 - 14.154\nu] \frac{P}{a^2} \qquad (5)$$

where P = applied load,

a = distance from the edge, and,

k = 7.2 - 14.154 ν

Equation (5) can now be used to predict the load at which the crack will start under the load. The implications of this are discussed in the next section.

3. Parametric Relationships

The anisotropic behavior of rocks is well known. Even in apparently uniform rocks like granite, the directionality of elastic and strength properties has been observed. However, to keep things simple, the following discussion is limited to homogeneous isotropic rocks. The effects of anisotropy are discussed in somewhat more detail in Appendix C. (q.v.)

TABLE B-1

BOUSSINESQ'S SOLUTION FOR ELASTIC QUARTER SPACE

Poisson's Ratio

Stress Along X Axis

	$z =$	0	0.1018	0.1758	0.2601	0.4383	0.7821	1.2781	2.0[illegible]	3.[illegible]
$\mu = 0$	$\sigma_x \frac{a^2}{p}$	0	0.0954	0.0[illegible]	0.1214	0.2024	1.2668	0.1[illegible]	0.[illegible]	0.[illegible]
	$\sigma_z \frac{a^2}{p}$	−0.3183	−0.1639	−0.1[illegible]	−0.0[illegible]	−0.0[illegible]	−0.1254	−0.[illegible]	−0.[illegible]	−0.[illegible]
$\mu = 1/6$	$\sigma_x \frac{a^2}{p}$	0	0.0751	0.0885	0.1756	0.3506	2.2403	1.4256	0.[illegible]	0.[illegible]
	$\sigma_z \frac{a^2}{p}$	−0.2122	−0.2240	−0.2[illegible]	−0.2[illegible]	−0.[illegible]	−2.2[illegible]	−1.[illegible]	−0.[illegible]	−0.[illegible]
$\mu = 0$	$\sigma_x \frac{a^2}{p}$	0	0.0585	0.1191	0.2296	0.3825	5.2851	2.0[illegible]	0.[illegible]	0.[illegible]
	$\sigma_z \frac{a^2}{p}$	−0.3183	−0.3368	−0.3[illegible]	−0.3[illegible]	−0.0[illegible]	−5.[illegible]	−2.0[illegible]	−0.[illegible]	−0.[illegible]

Poisson's Ratio

Stress Along Z Axis

	$z =$	0	0.1018	0.1758	0.2601	0.4383	0.7821	1.2781	2.0[illegible]	3.[illegible]
$\mu = 1/3$	$\sigma_x \frac{a^2}{p}$	−0.1061	−0.0350	0.0032	0.0279	0.1383	0.1518	0.0583	0.0[illegible]	0.0[illegible]
	$\sigma_z \frac{a^2}{p}$	0	0.0112	0.0102	0.0851	0.0812	−0.0211	−0.1436	−0.1421	−0.0779
$\mu = 1/6$	$\sigma_x \frac{a^2}{p}$	−0.2122	−0.1701	−0.1296	−0.0452	0.0379	0.0810	0.0620	0.0[illegible]	0.0[illegible]
	$\sigma_z \frac{a^2}{p}$	0	0.0045	0.0354	0.0733	0.0720	−0.0327	−0.1464	−0.1376	−0.0722
$\mu = 0$	$\sigma_x \frac{a^2}{p}$	−0.3183	−0.2891	−0.2585	−0.1714	−0.0438	0.0324	0.0465	0.0242	0.0[illegible]
	$\sigma_z \frac{a^2}{p}$	0	−0.0036	0.0286	0.0746	0.0118	−0.0330	−0.1527	−0.1319	−0.0712

TABLE B-2

PEAK σ_x STRESS AS PER HATEKYI SOLUTION

Poisson's Ratio	$a^2\sigma_x/P$	x/a
1/2	0.123	0.92
1/3	2.513	1.074
1/6	4.968	1.075
0	7.2	1.073

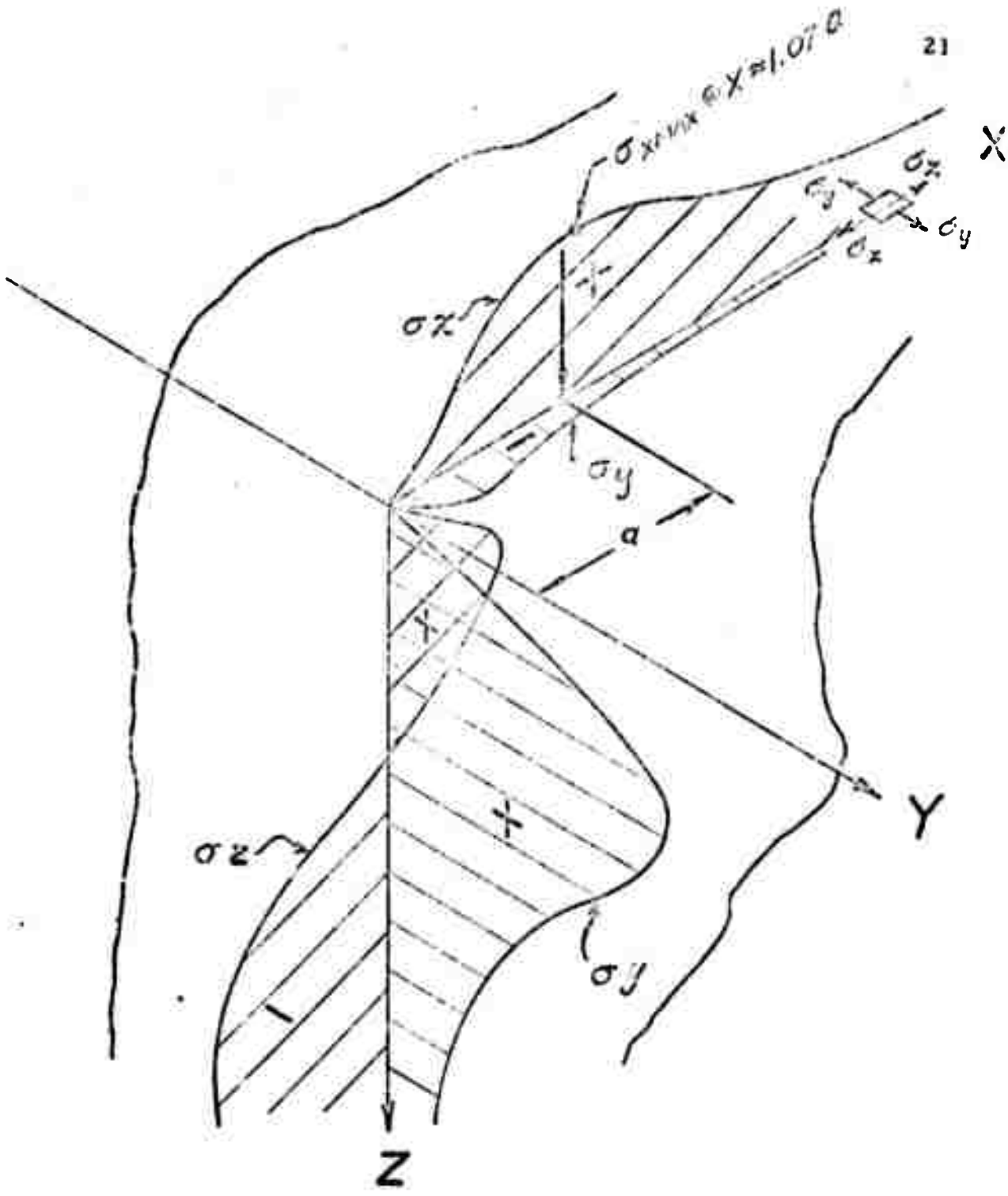

(STRESSES ALONG X AXIS AND Z AXIS)

Figure 8

STRESS DISTRIBUTION IN A QUARTER-SPACE

FIGURE 9

HATENYI'S SOLUTION

FOR $\sigma_{x_{max}}$

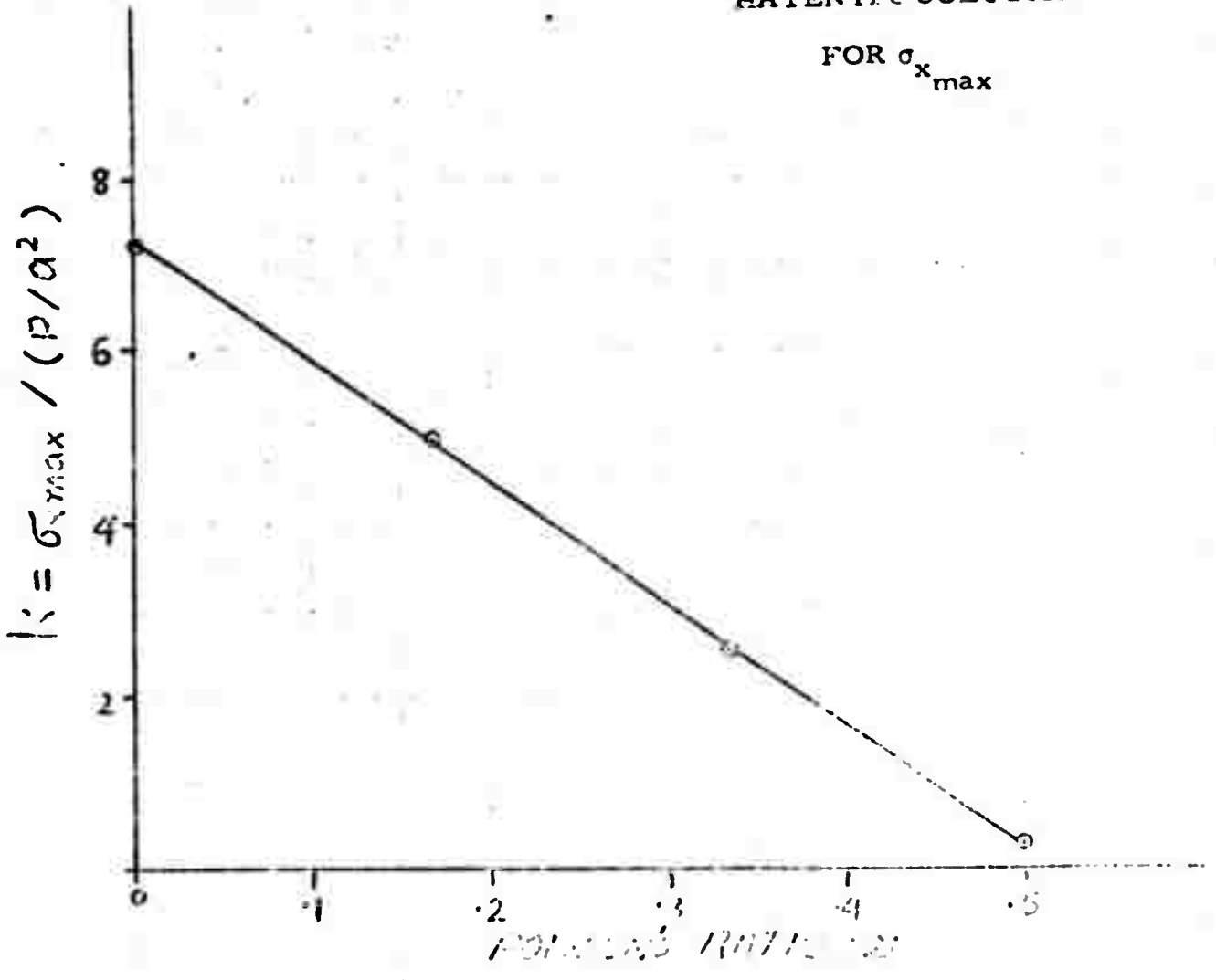

The indentation characteristics of moils on rocks are quite complex and should normally be obtained experimentally. However, Paul and Sikarskie obtained semi-empirical relations for wedge indentations, and Sikarski and Miller obtained these for a spherical-tipped conical indentor. In both cases, the details of chipping action of the tool are taken into account in arriving at the relationship between force and the indentation. These studies were oriented toward the percussive drilling problem, rather than impact fragmentation.

To arrive at a more simplified parametric relationship between the face, P, and blow energy, E, the following empirical expression will be used. Let the indentation be a function of the applied load.

$$\therefore E = \int_0^{\delta} P d\delta = \int_0^{P_{max}} P \frac{d\delta}{dP} dP \qquad (6)$$

We assume the functional relationship between P_{max} and E as follows:

$$P_{max} = cE^n \qquad (7)$$

where c and n are constants for a given pair of material and indentor. The values of c and n will depend on the mathematical model chosen to represent the indentative process. For example, consider the following:

(a) Parabolic spring approximation for a wedge-shaped indentation

$$P \propto \delta^2 \qquad (8a)$$

$$\therefore P \propto E^{2/3} \qquad (8b)$$

(b) Cubic spring approximation for pointed indentation.

$$P \propto \delta^3 \qquad (9a)$$

$$\therefore P \propto E^{3/4} \qquad (9b)$$

Other mathematical models can be used in a similar manner.

Using the general expression for equation (7), one can derive the expression for maximum stress of equation (5) as follows:

$$\sigma_{x_{max}} = \frac{kcE^n}{a^2} \qquad (10)$$

A single blow delivered at an energy level at which maximum σ_x just exceeds the tensile strength of the rock can cause a crack formation under the indentor in a direction normal to the x axis. This critical energy level is given by:

$$E_{cr} = \left[\frac{\sigma_t a^2}{kc}\right]^{1/n} \text{ lb-in.} \qquad (11)$$

Once the crack is started, it will be assumed to grow in the tensile stress region and reach the surface as shown in Figure 7a. Thus a roughly tetrahedral shaped piece of rock is produced by applying a single blow of energy E_{cr} to the rock. Further, it is reasonable to assume (from Fig. 7a):

$$b = c_1 a \qquad (12a)$$

$$h = c_2 a \qquad (12b)$$

where c_1 and c_2 are constants which must be determined experimentally.

The volume of roughly-tetrahedral shaped rock pieces (as shown in the figure) broken out is given by:

$$v = \frac{\lambda}{3}(2b)\frac{ha}{2} \qquad (13)$$

where λ is a shape factor. If one assumes a fracture curve approximating a parabola in the x-z plane, $\lambda \approx 2$. We will experimentally evaluate this parameter. From equations (12) and (13), it is clear that:

$$V = K_2 a^3 \qquad (13\text{-a})$$

For energy levels less than E_{cr}, the tool simply indents the rock and produces a small crater. The volume of rock crushed is very small in comparison with the roughly tetrahedral shaped volume of the rock fractured at $E = E_{cr}$.

If the blow energy is increased beyond E_{cr}, the volume removed is not increased at a given edge distance, a. Therefore one obtains a set of volume and energy characteristics for a given rock and tool as shown schematically in Figure 10. One can now write on the basis of equations (11) and (13-a) that the minimum value of critical energy is given in

$$\left(\frac{E}{V}\right)_{min} = \frac{K_3}{a^{3-(2/n)}} \qquad (13\text{-b})$$

4. Wedge-Shaped Moil

So far the discussion pertained to a pointed indentor. In this section we will examine wedge-shaped indentors. Figure 11 shows schematically the action of the indentor. Under the wedge a crater is formed. A crack which starts from the two opposite ends of the crater grows until it reaches the free surface. The chunk of rock thus broken out can be divided into two geometrical segments. The middle section is prismatic, and the two end portions similar to tetrahedra. If the width of the wedge becomes very small, the two end portions in principle will not be much different than those observed with pointed indentors (see Equation 13). This observation immediately leads to the following expression for the volume of rock broken:

$$V_w = \frac{\lambda}{3}(2b)\frac{ha}{2} + \frac{\mu}{2}wha = K_4 a^3 + K_5 a^2 w \qquad (14)$$

where V_w = volume of rock broken by wedge,

w = width of the wedge

b = $b_1 - \frac{w}{2} = b_2 - \frac{w}{2}$ = half width of the fractured rock (see Fig. 11)

h, a = have the same meaning as before (as shown in Figure 7)

λ, μ = constants to be determined experimentally

Another quantity one can obtain by simple comparison is the ratio of volumes broken by a wedge and a spherical indentor. Using equations (13) and (14), and re-arranging:

$$R = \frac{V_w}{V} = \frac{\left[\frac{\lambda}{3} 2bha + \left(\frac{\mu}{2}\right) wha\right]_{wedge}}{\left[\frac{\lambda}{3} 2bha\right]_{sphere}} \qquad (15)$$

One should not infer, at this stage, that the bigger volume produced leads

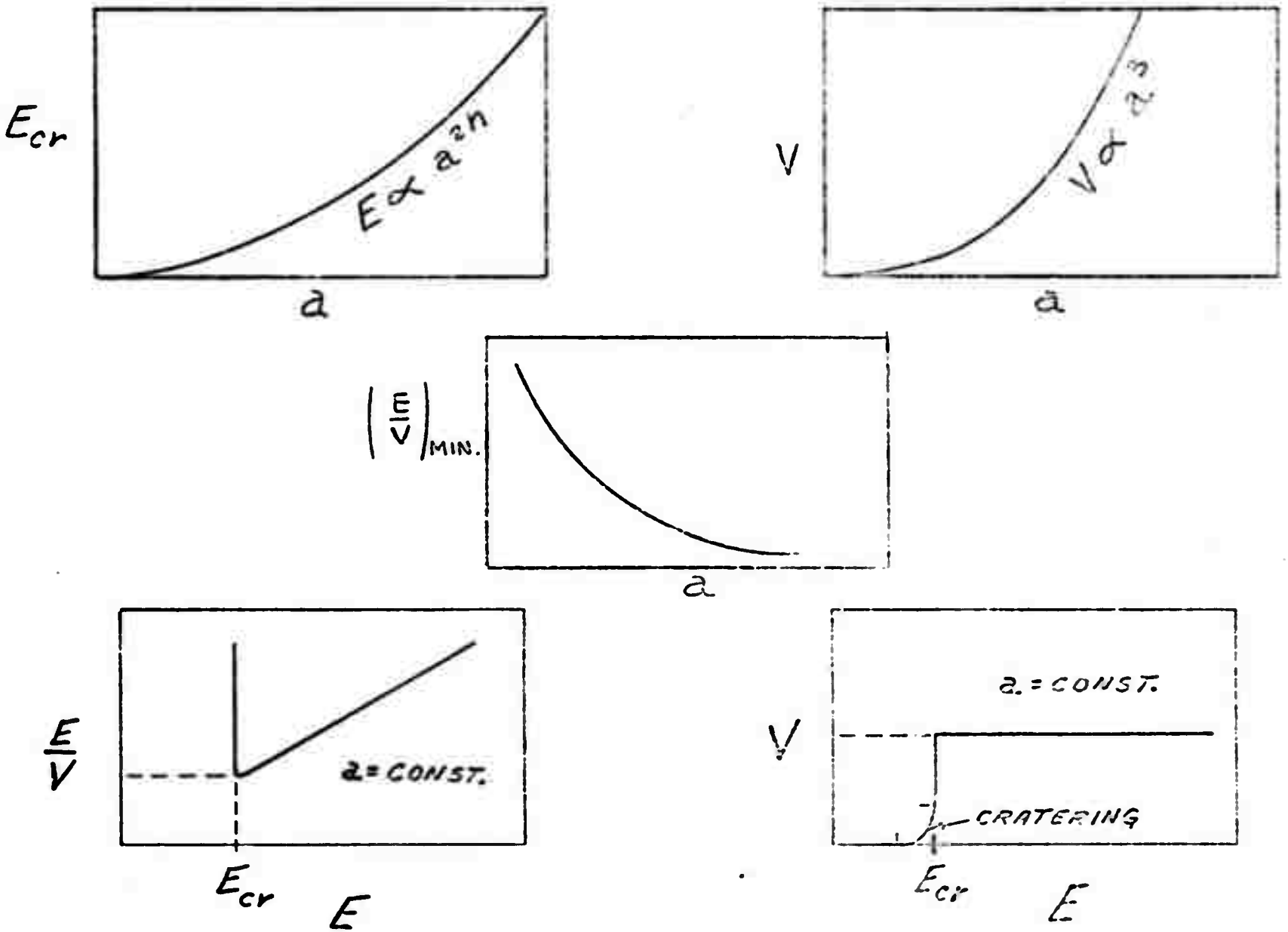

Figure 10: Energy, Volume and Edge Distance Relationships

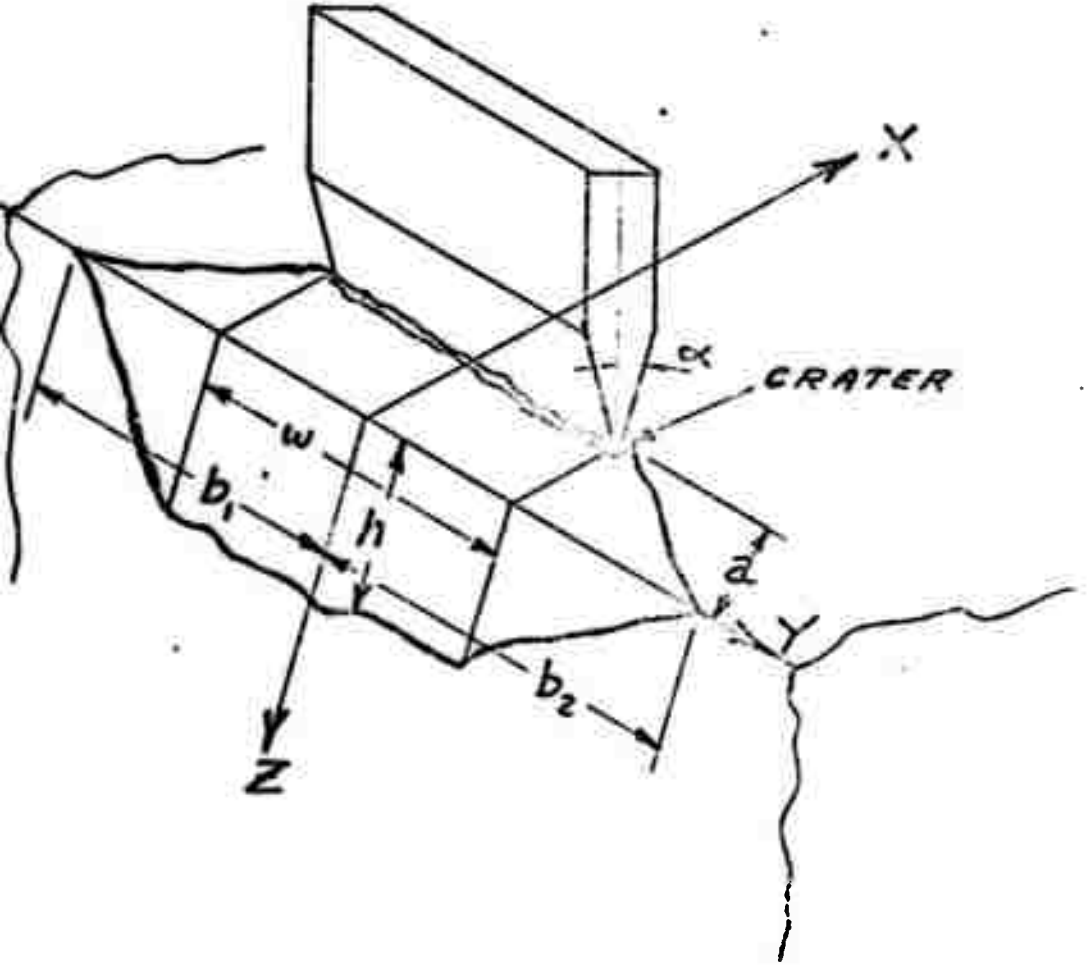

Figure 11a: Action of Wedge Shaped Moil

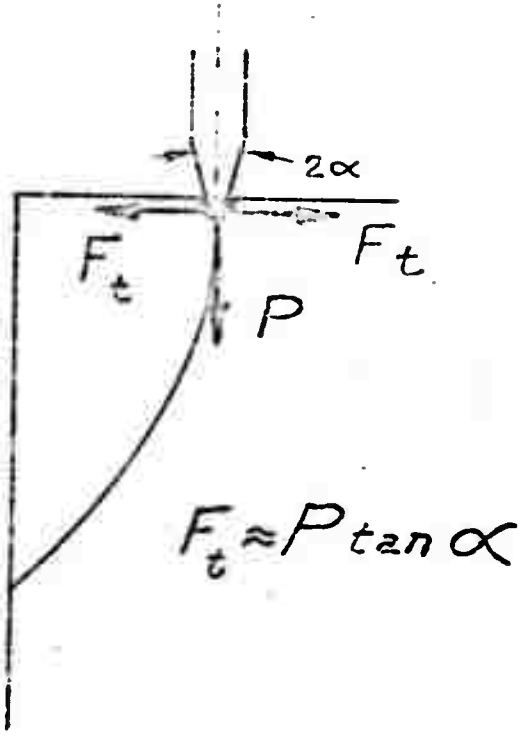

Figure 11b: Two-dimensional Idealization

Let $P = \frac{\bar{P}}{w}$ be the peak force applied per unit length of the wedge. The action of the wedge produces a tangential wedging force F_t, which is normal to $\bar{P}$. This force is far more effective in producing tensile stress than $\bar{P}$ itself. The solution for the line load F_t is again singular. However, we can write the simplified expression for the form of the stress as follows:

$$\sigma_{x_{max}} = \beta \frac{F_t}{a} = \beta \frac{P \tan \alpha}{wa} \tag{16}$$

where α = half-wedge angle.

Using the energy relationship $P = cE^m$, one obtains the critical energy in the following form.:

$$E_{cr-w} = \left[\frac{\sigma_t wa}{c \beta \tan \alpha} \right]^{1/m} \text{in. lb} \tag{17}$$

The constant, β, will be determined experimentally.

One must note that the two-dimensional approximation is valid for $w \geq a$. For $w << a$, the distinction between wedge and the pointed indentors should vanish. For our application , however, $w \approx a$.

5. Experimental Verification

The IRRI droptower facility was described in the semiannual report; a picture (Plate 11) is included here for reference. The experimental work was carried out by Messrs. C. Sliski and L. Yaros.

For the experiments, 18 in. Barre granite cubes were used. Each cube was suitably mounted under the droptower in such a way that the moil would impact at a desired distance, a, from the edge. The moil, an example of which is shown in Plate 12, can be raised to any desired height with the help of a hoist. After raising it to the desired height, it is released by a pneumatically actuated release mechanism. Aluminum guide collars and guide posts prevent side-to-side motion, tilting, and rotation of the

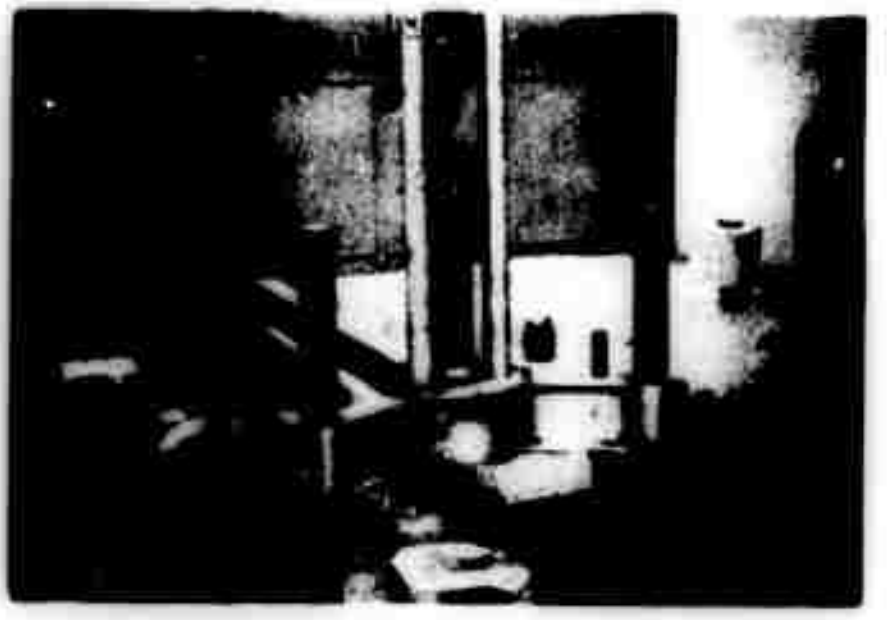

Plate 11: Droptower Facility

Plate 12: Moil and Point

moil as it comes down and hits the rock. The drop height (and hence the blow energy) was varied over a wide range in each case. Tool rebound was observed to be small. The directionality (bedding planes) could not be determined in all cases. Thus the results may be interpreted as averages taken over all directions.

A direct observation of critical energy (using probabilistic techniques) is very difficult without performing a large number of experiments. To keep the cost within limits and still allow a good estimate of critical energy, the following method was used. At each edge distance, a, the drop height was lowered to a point at which a single blow will usually not be able to cause edge fracture. Then tests were run at slightly higher energy levels where 60% to 80% of the times* a single blow will break out a chunk. This was then assumed to be the critical energy. In some cases estimates could be made only by using the experimenter's judgment.

(g) Spherical-tipped Moil

Three sets of experiments were conducted using a 5/8 in. diameter spherical-tipped moil at edge distances of 1/2 in., 1 in., and 2 in., respectively. Tables 1 through 3 in Appendix A show the blow energy, E, the number of blows, N, required to fracture the rock, the total blow energy (E x N), and the weight of the rock removed. In addition, the dimensions b_1, b_2, and h were measured for each broken piece of rock. It was observed that often b_1 and b_2 would not be equal due to a variety of reasons such as "bedding planes" being oblique to the edge, moil not hitting perfectly at right angle and inherent flaws in the rock. Tests in which $b_1 \approx b_2$ were judged to be more meaningful than when $b_1 \neq b_2$. To take this into account, a statistical weighting parameter was used in reducing the data. This weighting parameter, w, consisted of the ratio of the geometric mean to arithmetic mean, i.e.,

$$w = \frac{2\sqrt{b_1 b_2}}{b_1 + b_2} \qquad (18)$$

when $b_1 \approx b_2$, $w \approx 1$, and when $b_1 \ll b_2$ or $b_2 \ll b_1$, $w \approx 0$.

* The strength of rock in the direction normal to the bedding planes is larger than the other two directions. Thus on the average 1/3 of the times one should expect the rock not to break. Therefore we used a 60-80% limit.

In some instances, due to poor alignment, etc., one side of the fractures extended byond the block size, i.e., $b_1 \geq 9"$ or $b_2 \geq 9"$. These tests had to be discarded.

This statistical weight, w, was used to average b_1, b_2, and h, and the weight of the rock removed. The averages, means, and standard deviations were calculated in each case. Appendix B shows the results of statistical evaluation. In each case 95% confidence limits are calculated for each variable. In Figure 12 described below the means are shown by a circle and 95% confidence limit is shown by a bar.

Observations: Figure 12 shows the plots of the averages of b (it is the combined average of b_1 and b_2) and h. It is clear that except for a small offset, b and h are linear functions of a as expected by equations (12a and 12b). Our indentor was not a true pointed indentor but had a 5/16 in. radius, this probably caused the offset. The small offset in b and h leads to an error of 0.67 cu. in. in volume. When corrected for this error (by subtracting 0.67 cu.in. from measured volume), the averaged volumes of rock removed vary approximately as a cubic function of a as shown in Figure 13.

Figure 14 shows the log-log plot of the critical energies vs. edge distance. From the slope of the line passing through experimental data points, it was estimated that $E_{cr} \propto a^{1.84}$*.

Finally, Figure 15 shows the plot of specific energies in in. lb/in.^{3}, (psi). The slope of the curve clearly shows that the specific energy varies inversely as a, as one would expect from equation (13-b). In conventional tunnel boring practice, the specific energy is a sizable fraction of the compressive strength. In the case of edge fracture the specific energy is orders of magnitude smaller than the compressive and even the tensile strengths.

(b) Wedge-Shaped Moil

The experimental procedures used here were the same as above. The effect of wedge angle, although important, was beyond the scope of this work. It was, therefore, decided to drop the variation of the wedge angle and limit this year's experimental program to the determination of the important

---

* The first two points gave $E_{cr} \propto a^{2.14}$ or $n \approx 0.94$. This variation is probably due to the spherical radius at the tip of the pointed indentor.

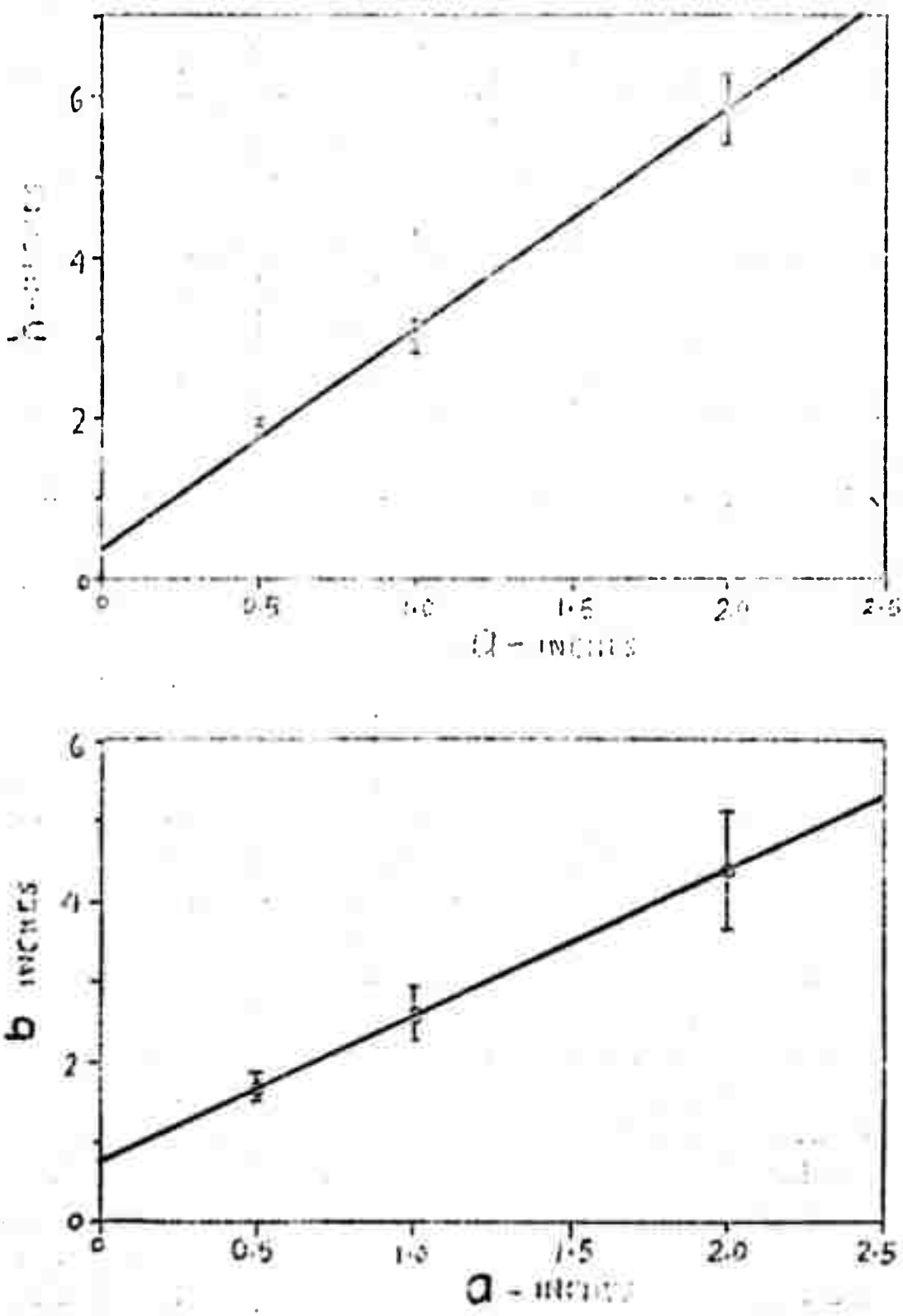

FIGURE 12: ROCK FRACTURE PARAMETERS
POINTED TOOL

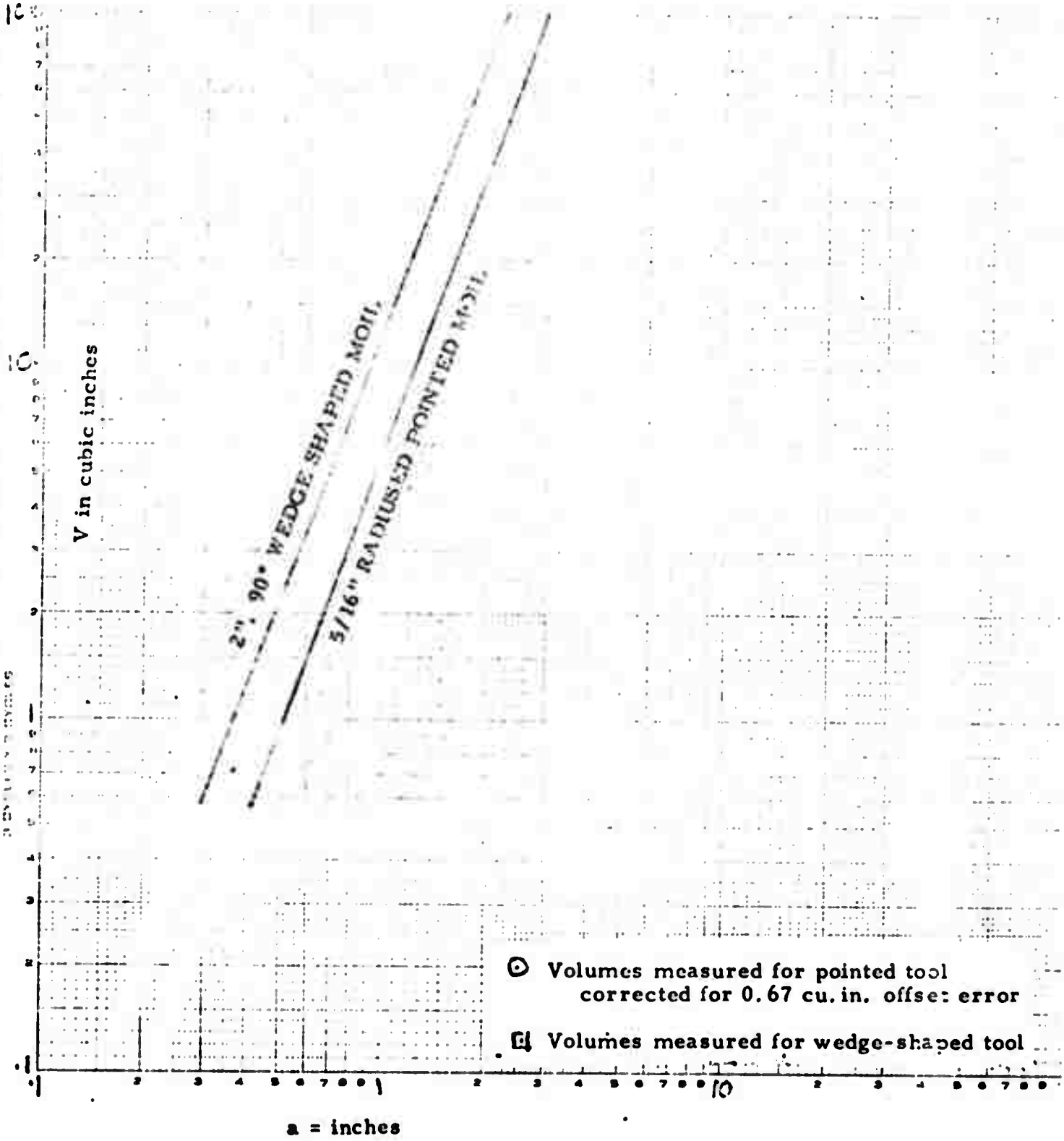

FIGURE 13: VOLUME OF ROCK REMOVED AS

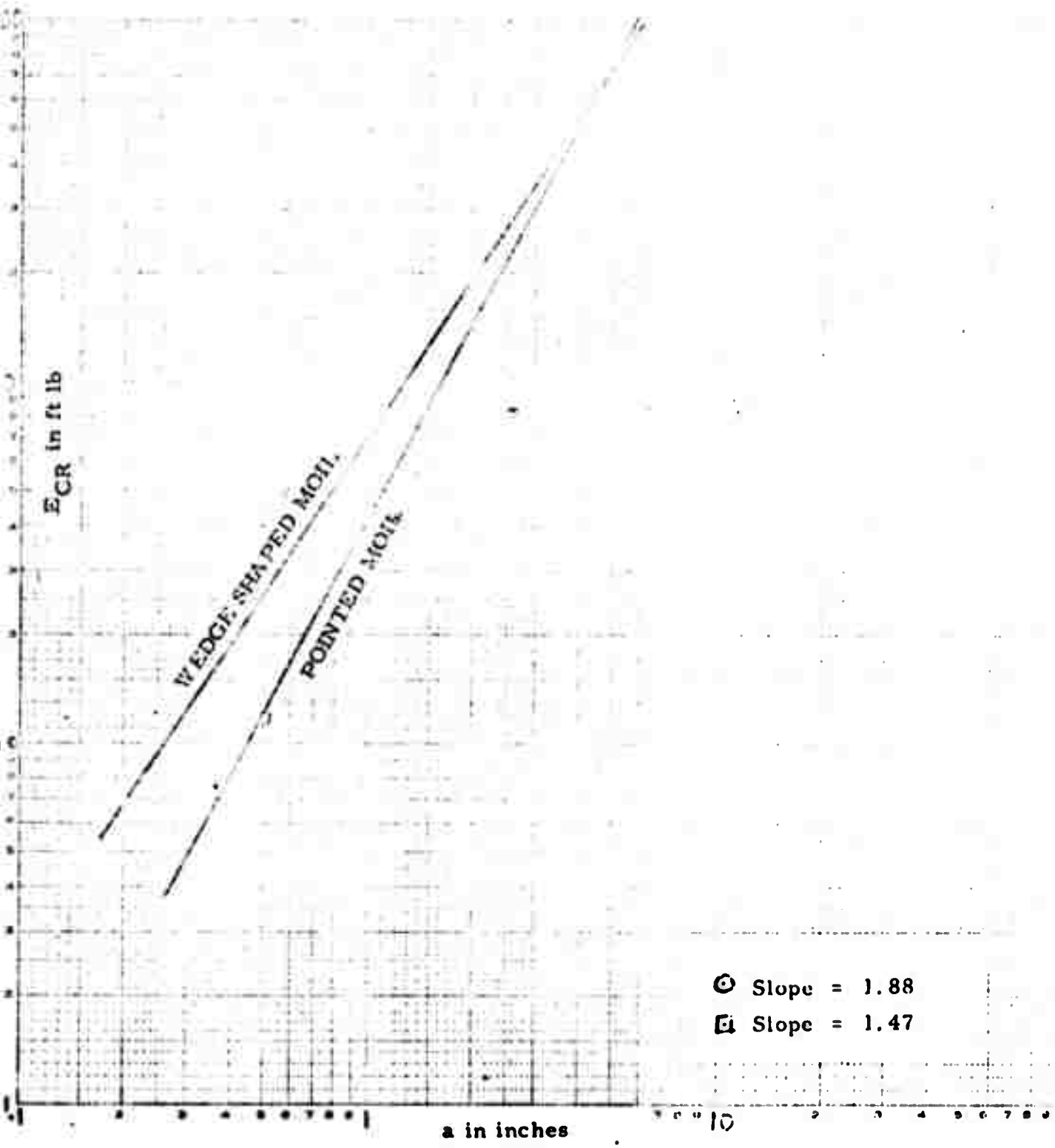

FIGURE 14: CRITICAL ENERGY AS A FUNCTION OF EDGE DISTANCE

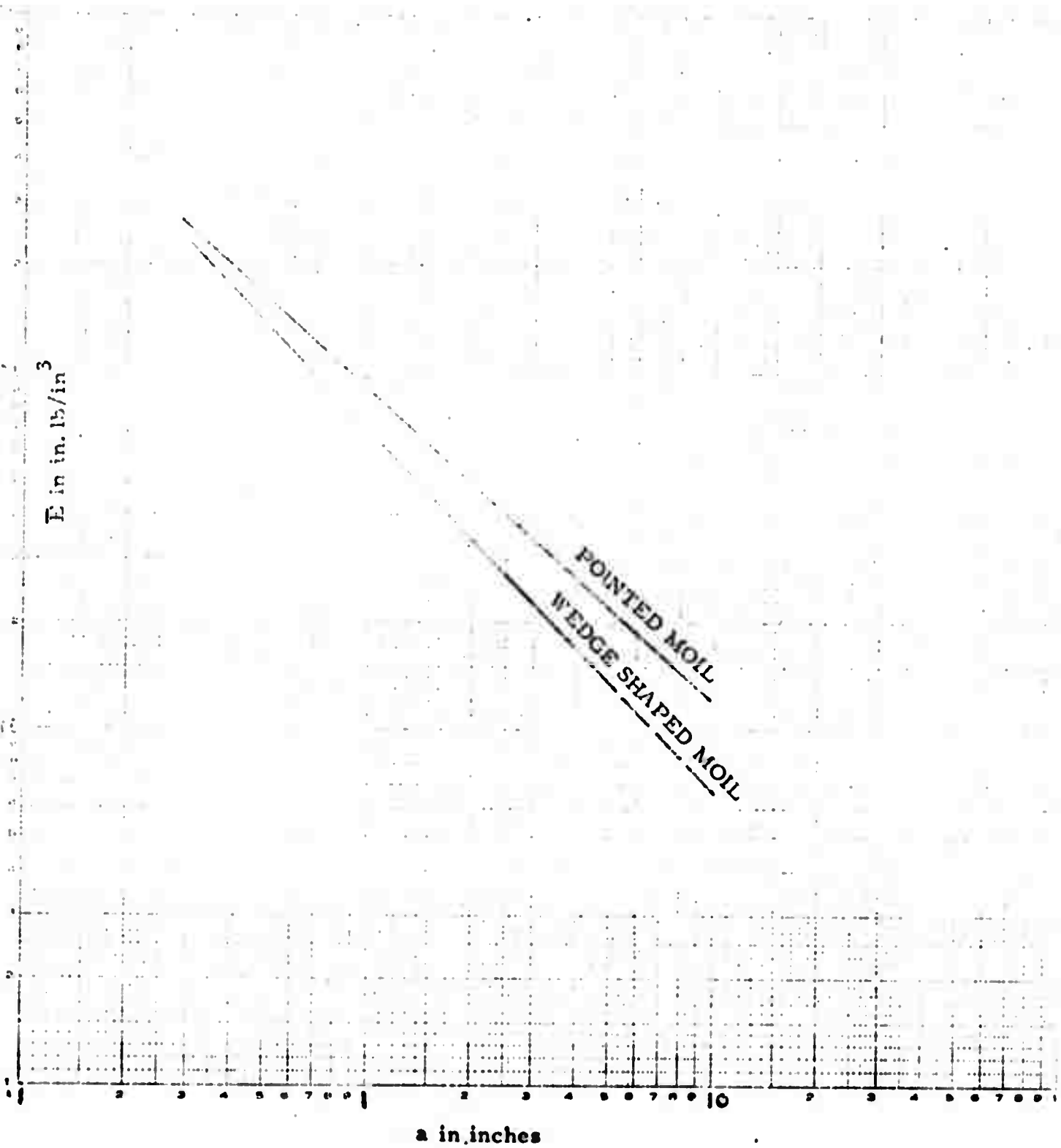

FIGURE 15: Specific Energy as a Function of Edge Distance

relationships between critical energy, volume of rock removed, and the edge distance, a. In all tests, a wedge of 90° included angle was used. The weighting functions used are the following:

$$w = \frac{2\sqrt{b_1^* b_2^*}}{b_1^* + b_2^*}$$

$$w = 0 \text{ when } b_1 > 0, \text{ or } b_2 > 0.$$

where $b_1^* = b_1 - \frac{w}{2}$

$$b_2^* = b_2 - \frac{w}{2}$$

Once again fractures breaking into one of the corners were discarded. However, it was found that even when the fractures progressed close to the corner (say within 1 to 2 in.) somewhat larger pieces were broken out than usual. In Figure 16 the plots of b vs a and h vs a are shown for the wedge. Notice in the plot of b vs a the point at a = 2 in. is well above what would be expected because of the proximity of the fracture to the corners. We therefore consider the dotted line passing through the three points erroneous and the solid line passing through the first two points to be the correct one. The weighted averages, means, standard deviations, confidence limits, etc. are obtained in the same manner as above (see Appendix B). Tables 4, 5, and 6 (Appendix A) show the summary of observations.

Figures 13, 14, 15, and 16 show the various relationships between the variables for the edge fracture problem.

6. Edge Fracture Conclusions

It is clear from the text that an understanding has been reached in the area of secondary fracture. The principal conclusions are as follows:

1. There exists a critical level of single blow energy at which a piece of rock breaks out from the edge.
2. The volume of rock broken out is principally a function of edge distance and tool shape.
3. Hatenyi's analysis can provide a basis for the crack initiation in edge fracture. More rock testing will be needed to prove the variation of critical energy as a function of tensile strength and tool wedge angle.

4. Basic geometrical relationships between b, h, V, and a derived in the text have been confirmed experimentally.

5. The 2 in. wedge-shaped tool proved to have lower specific energy than the pointed tool.

6. Low specific energies achieved during the tests hold a promise for tunneling system application.

7. Summary Results of the Edge Fracture Tests

The numerical relationships obtained for the set of tools and rock used during testing are given below:

Pointed tool: $b \approx 1.84a$; $V \approx 5.3a^{2.72}$; Specific Energy $\approx 96a^{-0.88}$

$h \approx 2.7a$; $E_{cr} \approx 42.5a^{1.84}$

2 In., 90° wedge tool: $b \approx 2.25a$, $h \approx 3.3a$; $V \approx 12.5a^{2.43}$

$E_{cr} \approx 70a^{1.47}$; Specific Energy $\approx 67a^{-0.96}$

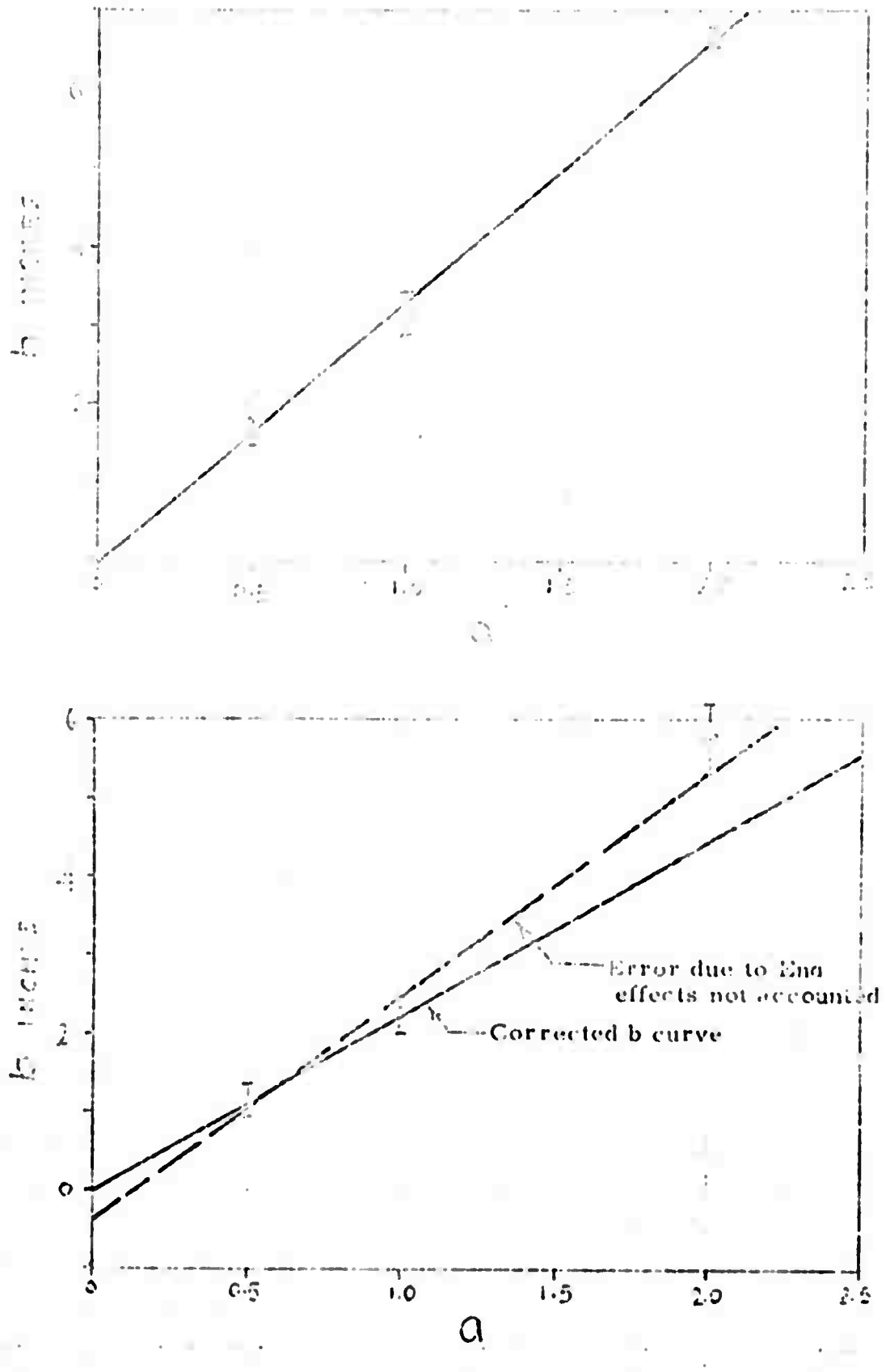

FIGURE 16: ROCK FRACTURE PARAMETERS FOR 2 IN. - 90° WEDGE

C. Field Tests

1. Introduction and First Field Test

The purpose of the field tests carried out during this program was to gain experience with in-situ impact rock excavation in hard extensive formations, utilizing available equipment.* To date, three field tests totaling six weeks duration have been carried out. Impactors capable of delivering 1000 ft lb/blow and 3000 ft lb/blow were available for all three field tests, while a 10,000 ft lb/blow impactor was available for the third test. The various moils used are shown in Plates 13 and 14.

The first field test was reported in the Semi-annual Report. At the time of the test, two impactors were available: a commercial 1000 ft lb/blow impactor, the Hobgoblin 1000, equipped with various steel moil points, and an experimental 3000 ft lb/blow impactor, the Demon 100, equipped with a blunt tool. The field test was conducted by C. Sliski who made the following observations:

(1) This test demonstrated that a wedge-shaped moil is more productive than a blunt or conical-shaped moil.

(2) The 3000 ft lb/blow impactor was more productive than the 1000 ft lb/blow impactor.

(3) Due to the high strength (compressive strength = 40,000 psi) diabase formation found at the quarry used, available tools could obtain only a limited amount of rock breakage off the face.

2. The Second Field Test

A second field test was conducted by C. Sliski during the period October 13-19, 1971 at the Shahmoon Industries Quarry in Mt. Hope, New Jersey. There is a granite gneiss formation in the quarry with rock properties as shown in Table C-1. Testing was done at a rock face which had a layered structure with a large number of small cracks along the rock layers. The following equipment was used: a standard Unihoe 117, a 1000

---

* TM-7111: "High Energy Impact Rock Breakage Research Program -- Semi-Annual Report," October 1971, p. 23.

ft lb/blow impactor with a stellite-coated wedge tool, a carbide button wedge tool, and a spade tool, and a 3000 ft lb/blow impactor equipped with a blunt point.

TABLE C-1

Compressive Strength	= 36,000 psi
Density	= 3.05 s.g.
Minerals	= Granite gneiss, having a major mineral constituent of Hornblende
Hardness	= 5 - 6 Moh

The brief experience with the several tools gave an indication as which tool would be better in terms of effective rock removal and longer wear. A blunt tool on the 3000 ft lb/blow impactor was not very effective in removing rock. We did not observe any subsurface cracks by visual inspection. The stellite-coated wedge tool lasts approximately twice as long as the basic wedge tool used previously. It, too, however, soon blunted and became ineffective. The carbide buttons on the carbide button tool broke quickly, and again the tool blunted to a large ineffective radius. The spade-shaped tool gave the most promising results. This tool has 1 in. thick blade , and therefore, as the tool wears the tip radius does not change much, and the shape of the tool is retained. (see Plate 13) This tool was the more effective of the tools and lasted through the tests.

The commercial Hobgoblin 1000 ft lb/blow impactor did not develop any operating problems while the experimental 3000 ft lb/blow impactor cracked at one of its welds. It produced only a large crushed rock zone beneath the blunt tool with which it was originally equipped. It was observed that this rock broke out more readily than the hard diabase rock of the first field test. C. Sliski estimated that 150 blows removed 158 pounds of rock from the face for a roughly-estimated specific energy of 142 psi. This removal was achieved by edge fracture using existing surface cracks.

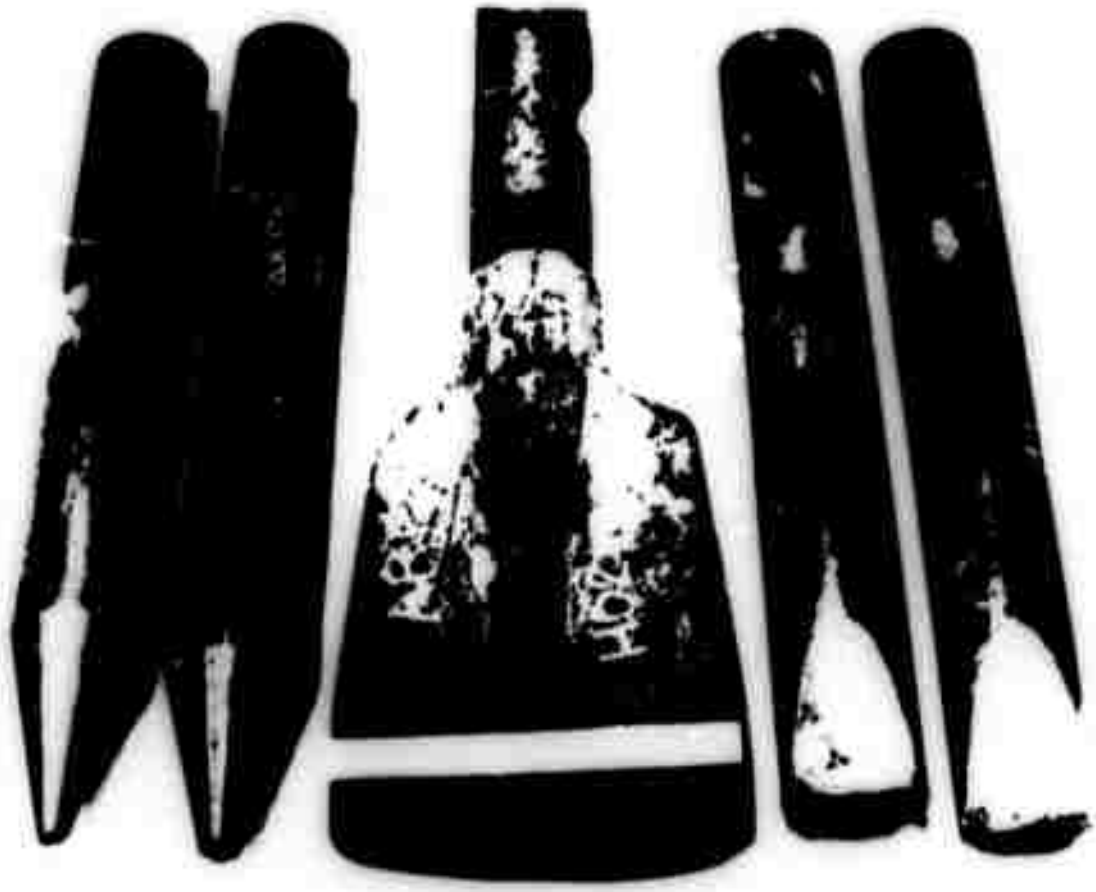

Plate 13: 1000 ft. lb. Impactor
Moil Points

(from left to right: cone, carbide ball tipped cone, spade, carbide ball tipped wedge, and steel wedge with 12 in. ruler shown on spade)

Several large boulders (approximately 4'x4'x4') were also used to test the impacting method. The boulders were solid and unweathered. The boulders were split with blows, both parallel and perpendicular to the favorable directions. With the Hobgoblin tool placed at the center of the rock, it was possible to split the rock with about 150 blows. A 1 in. deep crushed zone would form before splitting would occur. Once split, the rock could be broken further with more ease.

Some problems were encountered during the second field test. The Demon 100 hydraulic impulse breaker cracked at a weld before testing could be completed. The standard Unihoe 117 boom did not prove to be a good mounting for these impactors. The reflective shock from the blows resulted in broken hoses and lines. Also the rock removal rate was impeded by the awkward positioning of the impactor. Future impactor mountings should Provide for turning the impactor about its axis and changing its direction at a pivot point closer to the impactor.

3. The Third Field Test

A third field test was conducted by Lee Yaros during the period January 10 to February 14, 1972. The time spent in the field totalled about two weeks. During this time the weather was bad. On two occasions there were snow and ice storms preventing accessibility to the working face. The equipment consisted of a standard Unihoe 117 with the Demon 100 and Demon 300 impactors. These impactors were of 3000 ft lb/blow and 10,000 ft lb/blow energy respectively. The Demon 100 was equipped with a steel spade-shaped tool with a wedge-shaped point. Likewise the Demon 300 was equipped with a steel tool of the same shape as the previously-mentioned tool. The Demon 300 was also equipped with a carbide insert tipped tool with a wedge-shaped point (Plate 14).

The new spade-.and wedge-shaped tools were more effective than the blunt tools previously used on the 3000 ft lb/blow impactor. The tools produced smaller crushed rock zones, large pieces of rock were removed, and the crack direction could be determined by the operator. The steel points made of AISI 4340 steel showed minimal signs of wear. The carbide

Plate 14: 3000 and 10000 ft. lb. Impactor and Tools.

From top left to right: 3000 ft. lb. impactor with steel spade -wedge pointed tool; 10000 ft. lb. impactor with carbide tipped wedge tool, two blunt tools; and a steel spade -wedge pointed tool.

point on the 10,000 ft lb/blow impactor showed no signs of wear, chipping, or cracking after delivering 30 blows. The 10,000 ft lb/blow impactor was much more effective than the 3000 ft lb/blow impactor with chips of rock flying off with each blow. The operator had to protect himself from these flying chips. As a rough estimate, the 10,000 ft lb/blow impactor could effectively remove from a ledge in the face (in the secondary breakage mode), a 10 to 20 pound rock with a single blow indicating a specific energy of 71 to 142 psi. This unit is shown in Plate 15.

Some observations could be made from the third field test. The 10,000 ft lb/blow impactor was much more effective than the 3000 ft lb/blow impactor in producing secondary breakage. A movie sequence of the impactors operating in the secondary breakage mode has been made and forwarded to TCMRC. The tests were inconclusive in demonstrating the impactor's ability to produce primary cracks in this competent granite gneiss rock. The ability to see these cracks was hindered by the dirt, dust, mud, and water present on the rock face. The ability to induce crack interaction by geometric spacing of the blows was, likewise, inconclusive.

Several problems of a practical nature were encountered during the third field test. The four bolts used to hold the tool point onto the piston on the 10,000 ft lb/blow impactor broke. These four bolts were replaced by eight socket head bolts which lasted for the remainder of the tests. The Unihoe 117 boom could barely support the 10,000 ft lb/blow impactor due to its weight. To keep the machine from tipping over backwards, weight had to be added to the front bucket. The greatest problem encountered was the durability of the impactors. Both impactors cracked at various welds during the tests, stopping further tests.

4. Lab Field Tests - Five Foot Granite Cube

During early March, 1972, high energy impact rock breakage tests were carried out by L. Yaros on a five-foot Barre granite cube. The equipment used consisted of the Unihoe 117, the 3000 ft lb/blow impactor equipped with a spade tool, and the 1000 ft lb/blow impactor equipped with a blunted wedge moil and a carbide-tipped cone moil.

Plate 15: Field test of [illegible] ft. lb. Impactor in Greater [illegible] near Mt. Hope, New Jersey.

Test one consisted of some edge fracture tests using the 3000 ft lb/blow impactor. The results are given in Table C-2 below.

TABLE C-2

Sequence Number	a	Number of blows	Weight of Rock Removed	Specific Energy
1	<3"	1	7 lb.	494.0 psi
2	3"	1	13 lb.	265.0 psi
3	>3"	2	162 lb.	52.5 psi
4	5"	4	131 lb.	105.0 psi

Figure 17 shows the position of the pieces of rock removed during the test. This test gave confidence that the data obtained on the drop tower yields reasonable quantitative estimates. No effort was made to determine critical energy and specific dimensions of breakage.

Test two was to determine the effect of closely spaced blows at 3000 ft lb. blow energy (see Figure 18).

Blows of 3000 ft lb were delivered at the center of the block within the two foot circle in a random fashion. Some of the blows were delivered parallel to side A, others were delivered parallel to side B.

TABLE C-3

Sequence Number	Number of Blows	Blow Parallel to Face
5	7	A
6	8	A
7	10	B
8	10	B
9	20	B

After each sequence of blows, the rock surface was cleaned with a wire brush, and an attempt was made to find some cracks. Although no visible primary cracks were observed, a crater 2 ft in diameter and approximatel

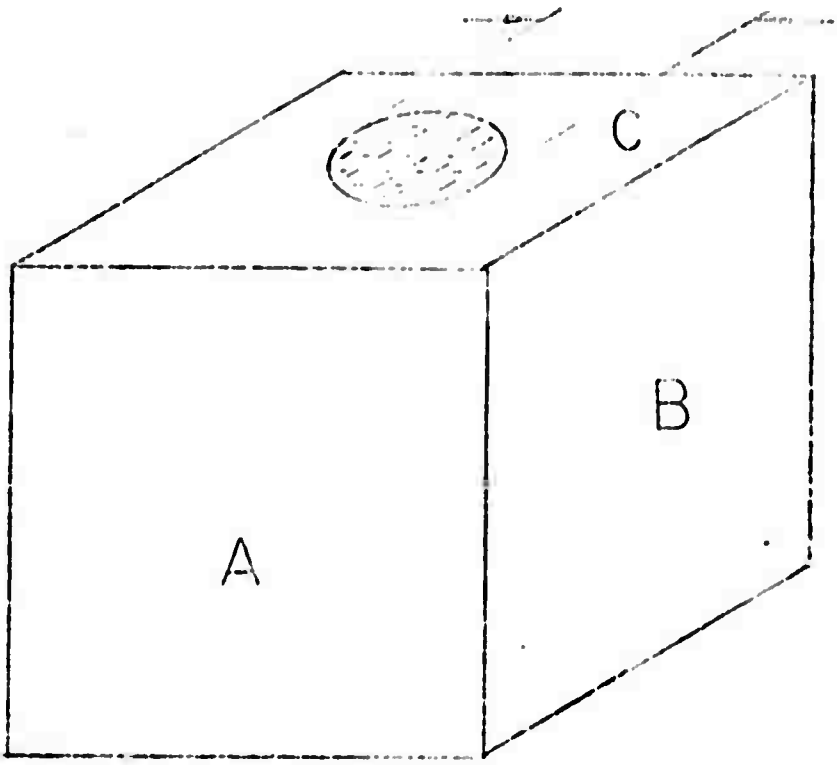

FIGURE 17: PRIMARY FRACTURE TESTS - 5 FT BARRE GRANITE CUBE

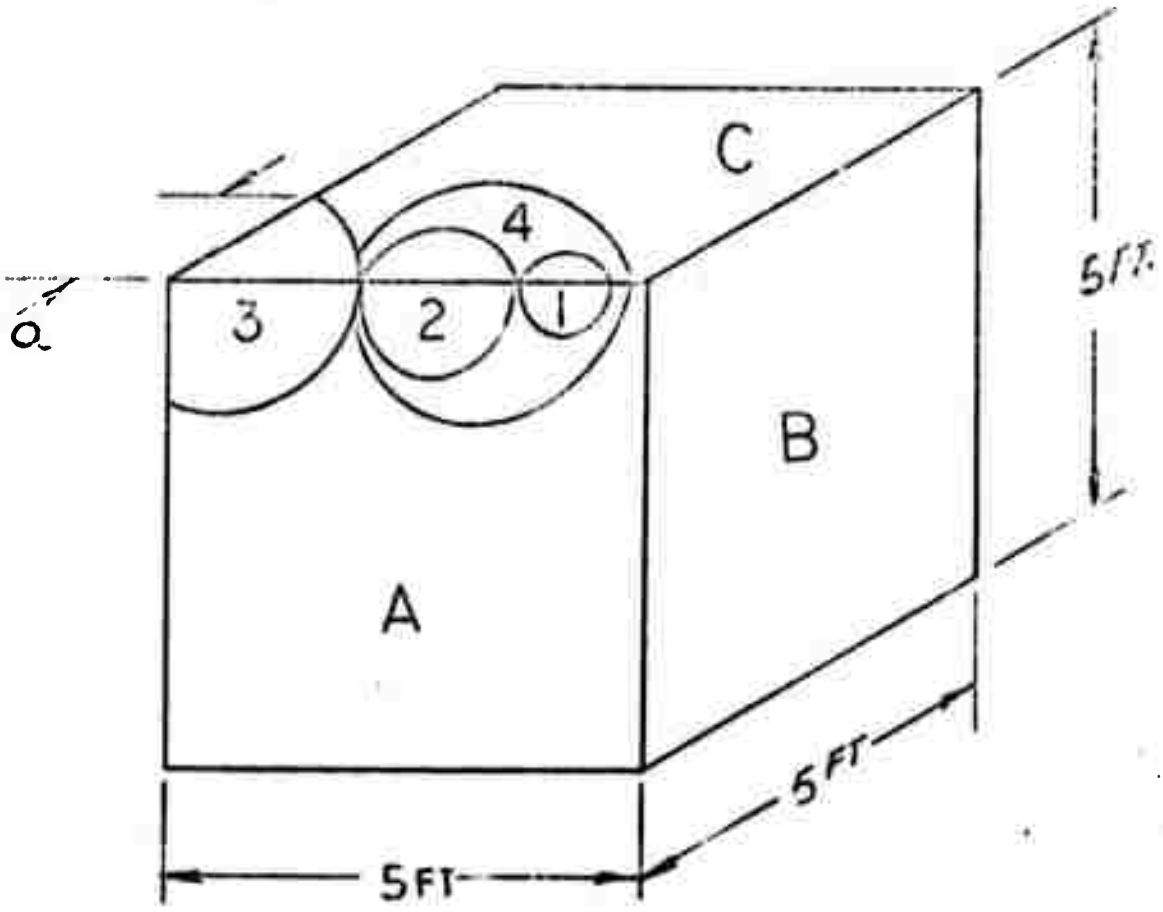

FIGURE 18: SECONDARY FRACTURE TESTS - 5 FT BARRE GRANITE CUBE

1 in. deep was formed in the cube by the removal of 1/2 in. to 1 in. chips of rock. From these rough estimates, a specific energy removal rate of 4370 psi was estimated.

During the last sequence of tests, the 3000 ft lb/blow impactor cracked at its welds.

With the experimental 3000 ft lb/blow and 10,000 ft lb/blow impactors both damaged, an attempt was made to use the commercial 1000 ft lb/blow impactor to impact a five-foot cube granite block with carbide-tipped cone and wedge moils. At this low energy the moils pulverized the rock instead of removing chips and were therefore ineffective. (A roughly estimated specific energy removal rate of 32,000 psi was obtained when the 1000 ft lb/blow impactor was operated for one-half hour with blows randomly spaced within the two foot circle.)

5. Field Test Conclusions

1. A spade-shaped tool is better than other shapes because the crack direction can be controlled by the operator, and its wear characteristics are better than other shapes.

2. Secondary breakage rock removal could be done effectively with the equipment available.

3. Primary cracks could not be readily observed during the field tests, and proof of our ability to induce them with the field test equipment available is inconclusive.

4. The higher the blow energy available, the more effective the impactor from the standpoint of rock removal rate.

III. FIELD TEST PROBLEMS

The problems generally encountered throughout the tests were mainly concerned with the maneuverability and durability of the equipment used. As has been mentioned previously, the boom on the standard Unihoe 117 does not readily allow accurate and easy positioning of the impactors, nor can it handle the shock of the impacting blows. However, durability of the experimental impactors was the major problem encountered. Had the 3000 ft lb/blow and 10,000 ft lb/blow impactors been able to withstand the punishment of the tests longer, a small tunnel could have been made in the quarry face at Mt. Hope, N.J. This would have allowed us to make overall specific energy measurements and would have indicated that primary cracks were being induced in the rock.

IV. FUTURE PLANS

At the end of the first year the following comments may be made with the view of applying high energy impact tools to a practical tunneling system.

(a) Rather substantial blow energy is required to create large subsurface cracks. For example, the theoretical work indicates that a 10,000 ft lb tool (8 in. long, wedge-shaped) would create a crack 10 in. to 12 in. deep in granite. This is probably just into the lower end of the practical range of application. In harder rocks larger impact tools will be needed.

The tests also showed that a wedge-shaped tool was better than a pointed or blunt tool.

(b) Secondary fracture showed the promise of high energy impact breakage to attain low specific energy in tunneling. Here also the wedge-shaped tool was found to be better than the spherical-tipped pointed indentor.

(c) The field testing showed a need for a more reliable impactor and a better mounting to obtain maneuverability for the high blow energy tools.

Plans for the Second Year

The second year as planned ends in December 1972, and thus has a duration of eight months. To utilize the time most effectively, it is planned to concentrate work in three basic areas, namely:

(a) to re-design the 10,000 ft lb impact tool.
(b) to perform pertinent rock testing with rebuilt equipment as needed.
(c) to examine some interactive considerations of strategy and mountings in order to design the tool.

Field testing with available tools, although useful, is not contemplated for this year due to lack of a reliable tool in the useful blow energy range. However brief tests may be carried out to gain design information.

It is suggested, therefore, that the work should be divided roughly as follows:

Item	% of Resources
10,000 ft lb tool, re-design and rebuild	60%
Sizing 50 000 ft lb tool	20%
Rock testing and tool-shape testing	20%

The design effort should include consideration such as whether to use impacting piston type or hurled-bit type device, what structure must be used to support the tool, and the basic hydraulics of the system. Weak links* observed in the system during field test must be eliminated. The tool design work will be done in consultation with Impulse Products Corporation, and Prof. Voitsekhovsky in the U.S.S.R.

Rock testing should be done in a different rock then granite. Suitable rock will be chosen, and after approval of the Bureau of Mines, 30 blocks of 1-1/2 ft cube will be obtained. Ten blocks will be used to determine subsurface fracture, and twenty blocks will be used for edge fracture.

Finally some thought would be given to available mountings and secondary systems. In particular, the available crawler mountings will be studied to estimate changes needed in these for future field trials of 10,000 ft lb tools.

The outline of this proposal effort has been forwarded to TCMRC for approval.

---

* These include (1) welded joint failures at the side restraint due to side loads. (2) automatic recycling, (3) bending and transverse load failure of the tool point.

V. REFERENCES

1. Fairhurst, C. and W. D. Lorimer. "Some Principles and Developments in Hard Rock Drilling Technique." Proceedings Sixth Annual Drilling and Blasting Symposium, University of Minnesota. (October 11-13, 1956), pp. 1-25.

2. Reichmuth, D. R. "Correlation of Force-Displacement Data with Physical Properties of Rock for Percussive Drilling Systems." Rock Mechanics. Proceedings of Fifth Symposium on Rock Mechanics, Edited by C. Fairhurst, University of Minnesota, Pergamon (1963), pp. 33-61.

3. Paul, B. and D. L. Sikarskie. "A Preliminary Theory of Static Penetration by a Rigid Wedge into Brittle Material." AIME Transactions (1965) pp. 372-385.

4. Miller, M. H. and D. L. Sikarskie. "On the Penetration of Rock by Three-Dimensional Indentors." Intl. J. of Rock Mechanics and Mining Sciences, (1965), pp. 375-390.

5. Paul, B. and M. D. Gangal. "Why Compressive Loads on Drill Bits Produce Tensile Splitting in Rock." Paper No. SPE2394, (1969).

6. Aquino, C. F. "Prediction of Fractures Due to a Hammer Striking a Brittle Half Space." (February, 1971), Private communication from Bell Labs.

7. Hoilenberg, Joel W., Chester J. Sliski, and Mukund D. Gangal. "High Energy Impact Rock Breakage Research Program Semi-Annual Report." (October, 1971). Sponsored by Advanced Research Projects Agency. Bureau of Mines Contract No. H0220045.

8. Simon, R., D. E. Cooper, and M. L. Stoneman. "The Fundamentals of Rock Drilling." Presented at Spring Meeting of Eastern District of API, Divn. of Production, Columbus, Ohio. April 25-27, 1956.

9. Hartman, H. L. "Simulation of Percussion Drilling in the Laboratory by Indexed Blow Studies." Proceedings of the 1st Conference on Drilling and Rock Mechanics, University of Texas, (1963).

10. Garner, N. E. "The Photoelastic Determination of the Stress Distribution Caused by a Bit Tooth on an Indexed Surface." M.S. Thesis, University of Texas, (January 1961).

11. Evans, I. and S. Murrell: "The Forces Required to Penetrate a Brittle Material with a Wedge Shaped Tool." Mechanical Properties of Non-Metallic Brittle Materials. Interscience Publications. (New York, 1958).

12. Hatenyi, M. "A General Solution for Elastic Quarter Space." J. Appl. Mech. (March, 1970). pp. 70-76.

13. Hatenyi, M. "A Method of Solution for the Elastic Quarter Plane." J. Appl. Mech. (June 1960), pp. 289-296.

APPENDIX A

Tables 1 through 6 give the summary of observations made during the drop tower testing for edge fracture. Blow energy is in ft lb and the weight of the rock removed is in pounds.

Table	a	Tool
1	$\frac{1}{2}$ in.	Spherical, 7/16" dia.
2	1 in.	Spherical, 7/16" dia.
3	2 in.	Spherical, 7/16" dia.
4	$\frac{1}{2}$ in.	90° Wedge, 2 in. long
5	1 in.	90° Wedge, 2 in. long
6	2 in.	90° Wedge, 2 in. long

Quantities b, h, and volume, and the statistical evaluation can be found in Appendix B. Determination of the critical energy has been explained in the test in subsection 5 of the chapter on Edge Fracture.

TABLE 1

SUMMARY OF DROP TOWER TESTS 1

RUN NO.	BLOW ENERGY	NO. OF BLOWS	TOTAL BLOW ENERGY	WEIGHT OF ROCK REMOVED
163	7.92	2	15.84	0.113
164		3	23.76	0.194
165		2	15.84	0.163
167		2	15.84	0.152
168		2	15.84	0.0883
170	11.9	2	19.82*	0.245
171		2	23.8	0.155
174		1	11.9	0.0707
172		1	11.9	0.146
162		1	11.9	0.0706
154	47.5	1	47.5	0.157
155		1	47.5	0.258
156		1	47.5	0.181
157		1	47.5	0.121
158		1	47.5	0.197

* Smaller Second Blow.

TABLE 2

SUMMARY OF DROP TOWER TESTS II

RUN NO.	BLOW ENERGY	NO. OF BLOWS	TOTAL BLOW ENERGY	WEIGHT OF ROCK REMOVED
150	31.4	1	31.4	0.25
152		1	31.4	0.25
149		2	62.8	0.75
153		2	62.8	0.50
148		2	62.8	0.70
143	47.5	1	47.5	0.75
141		1	47.5	0.50
140		1	47.5	0.65
142		2	95.0	0.60
144		1	47.5	0.75
133	95.0	1	95.0	0.35
132		1	95.0	1.00
135		1	95.0	1.50
137		1	95.0	0.25
136		1	95.0	0.50
138		1	95.0	0.25
139		1	95.0	0.35

TABLE 2

SUMMARY OF BLOW TORCH TESTS [illegible]

RUN NO.	BLOW ENERGY	NO. OF BLOWS	TOTAL BLOW ENERGY	WEIGHT OF ROCK REMOVED
9	1045	1	1045	4.0
10	1045	1	1045	11.0
12	238	1	238	3.0
13	238	9	1711.5	14.0
41	238	1	238	5.5
42	190	1	190	4.0
43	143	1	143	1.0
44	143	4	572	7.0
45	143	1	143	2.5
46	143	1	143	1.5
47	143	1	143	3.0
48	190	9	428	12.0
49	95	3	285	6.5
50	95	5	475	3.5
51	95	3	285	6.5
52	95	2	190	1.5
54	238	1	238	1.2
55	238	2	476	12.0
56	238	2	476	1.15
57	238	1	238	8.5
58	238	3	574	3.5
59	238	1	238	2.75
60	574	3	238	1.75
61	520	1	520	4.5
62	520	1	520	0.465
63	520	1	520	3.0
64	520	1	520	8.5

TABLE 4

SUMMARY OF DROP TEST DATA IV

RUN NO.	BLOW ENERGY	NO. OF BLOWS	TOTAL BLOW ENERGY	WEIGHT OF ROCK REMOVED
175	19.0	2	38.0	0.318
184		2	38.0	0.298
185		1	19.0	0.086
186		5	95.0	0.195
189		2	38.0	0.324
177	25.4	2	50.8	0.115
178		5	127.0	0.239
180		1	25.4	0.152
181		1	25.4	0.177
182		1	25.4	0.174
183		2	50.8	0.106
176	38.0	1	38.0	0.130
190		1	38.0	0.287
191		1	38.0	0.422
192		1	38.0	0.186
193		1	38.0	0.161

TABLE 5

SUMMARY OF DROP TOLIT TESTS V

RUN NO.	BLOW ENERGY	NO. OF BLOWS	TOTAL BLOW ENERGY	WEIGHT OF ROCK REMOVED
127	39.6	6	316.8	1.75
128		5	237.6	1.25
130		2	79.2	0.8
126		7	316.8	0.5
125		3	118.8	0.6
107	48.5	1	48.5	1.0
109		2	97.0	2.0
110	52.8	3	184.8	1.25
124	79.2	1	79.2	1.40
123		2	214.2	1.50
122		1	79.2	0.8
121		1	79.2	0.8
120		1	79.2	1.25
113		2	158.4	2.25
112		4	316.8	1.0
129		1	79.2	0.6
114	118.8	1	118.8	1.2
115		2	237.6	0.7
116		1	118.8	2.0
117		1	118.8	1.0
118		1	118.8	1.2
119		1	118.8	1.0
131	316.8	1	316.8	1.25
134		1	316.8	1.5

TABLE 6

SUMMARY OF DROP TEST RESULTS VI

RUN NO.	BLOW ENERGY	NO. OF BLOWS	TOTAL BLOW ENERGY	WEIGHT OF ROCK REMOVED
95	145.5	1	145.5	6.0
83		2	194.0*	7.25
82		2	194.0	6.0
79		2	194.0	11.0
86		3	339.5	9.5
85		3	339.5	8.25
80		2	194.0	8.5
81	194.0	1	194.0	6.75
78		1	194.0	6.5
76		1	194.0	6.5
75		1	194.0	8.0
74		1	194.0	8.5
87		2	242.0	6.25
77		1	194.0	6.5
88	238.0	1	238.0	4.5
89		1	238.0	8.5
90		1	238.0	10.0
91		1	238.0	10.0
92		1	238.0	10.0
93		1	238.0	9.0
94		1	238.0	10.0
73		1	238.0	7.0

* Multiple blows: each blow of the set of blows is not necessarily of equal magnitude.

APPENDIX B

A short computer program was written to determine averages, means, standard deviations of the quantities b_1, b_2, b, h, and w using the weighing functions described in the text.

The output first lists all the measured values of b_1, b_2, h, and weight of rock removed during each test with the pointed and wedge-shaped indentors and then shows the statistics --i.e., averages, means, and standard deviations in each variable. Interpret B1 as b_1, B2 as b_2, H as h in the printout. The 95% confidence limits imply that one has a 95% confidence that the true average of the global sampling will fall within these limits obtained from the experimental data. These limits are not shown in the attached printout but were calculated and used in preparing Figures 12 and 16 in the text (plots of b and h vs a).

PRINTED INVENTORY TESTS- STATISTICAL ANALYSIS

ITEM NO.	DEMAND	A	B	C	D	E
	U.N.B.	IN.	IN.	IN.	IN.	IN.
163	15.000	.500	1.750	1.750	1.500	.125
160	23.750	.500	2.000	1.500	2.000	.250
165	15.000	.500	2.750	1.000	2.000	.250
167	15.000	.500	2.500	1.000	2.000	.250
168	15.000	.500	1.250	1.000	1.250	.250
170	19.000	.500	1.500	1.000	2.000	.250
171	23.000	.500	2.000	1.000	1.750	.125
174	11.500	.500	1.500	1.000	1.000	.063
172	11.500	.500	1.500	1.000	1.000	.125
162	11.000	.500	1.500	1.000	1.000	.063
154	47.000	.500	1.000	1.000	1.000	.125
155	47.500	.500	2.000	1.000	2.000	.250
156	47.500	.500	2.000	1.000	2.000	.125
157	47.500	.500	1.500	1.000	2.000	.125
152	47.500	.500	1.750	1.000	2.000	.125
150	31.000	1.000	1.000	1.000	1.000	.250
152	31.000	1.000	2.000	1.000	2.000	.250
149	62.000	1.000	3.000	2.000	1.000	.750
153	62.000	1.000	3.000	2.000	2.000	.500
148	62.000	1.000	3.250	1.000	2.000	.750
143	47.500	1.000	2.000	1.000	2.000	.250
141	47.500	1.000	3.000	2.000	2.000	.500
140	47.500	1.000	3.500	1.000	3.000	.250
142	95.000	1.000	1.000	3.750	3.500	.000
144	47.500	1.000	2.750	3.000	3.000	.750
133	95.000	1.000	2.000	2.000	3.000	.250
132	55.000	1.000	3.500	3.000	3.000	1.000
135	95.000	1.000	3.000	3.750	4.000	1.500
137	95.000	1.000	2.500	1.250	2.750	.250
136	95.000	1.000	1.500	3.750	2.750	.500
138	95.000	1.000	1.750	1.750	2.000	.250
139	95.000	1.000	3.250	1.500	2.750	.250
47	143.000	2.000	6.000	5.500	5.500	3.000
46	143.000	2.000	4.000	3.000	2.500	1.500
45	143.000	2.000	3.000	6.000	5.000	2.500
43	143.000	2.000	1.250	2.500	3.750	1.000
42	190.000	2.000	7.000	7.000	7.000	4.000
41	238.000	2.000	4.000	7.000	7.000	5.500
54	238.000	2.000	1.500	2.500	6.500	1.200
57	238.000	2.000	8.000	4.500	9.000	8.500
59	238.000	2.000	6.000	4.000	4.000	2.750
12	238.000	2.000	2.250	6.000	6.000	3.000
11	523.000	2.000	9.000	9.000	6.000	6.500
61	523.000	2.000	5.000	7.000	6.500	4.500
62	523.000	2.000	2.500	1.000	4.000	.500
63	523.000	2.000	4.000	7.000	6.500	3.000
64	523.000	2.000	2.500	9.000	11.000	8.500
10	523.000	2.000	1.500	9.000	9.500	11.000
9	1045.000	2.000	5.000	2.750	6.000	4.000
52	1045.000	2.000	4.000	2.250	4.250	1.500
51	190.000	2.000	5.000	7.000	6.000	6.500
50	385.000	2.000	4.500	2.000	8.000	3.500
49	385.000	2.000	4.500	5.000	4.500	6.500
48	385.000	2.000	9.000	8.000	8.000	12.000
44	385.000	2.000	6.000	7.000	9.000	7.000
55	476.000	2.000	9.000	9.000	6.500	12.000

POINTED INSULATOR TESTS- STATISTICAL

RUN NO.	F [illegible] FT.LB.	A IN.	B IN.	[illegible]	[illegible]	[illegible]
58	714.000	2.000	6.500	[illegible]	[illegible]	3.500
60	714.000	2.000	2.750	[illegible]	[illegible]	[illegible]
14	714.000	2.000	9.000	[illegible]	[illegible]	[illegible]

14	31,000	1.000	2.500	2.750	1.875	.313
15	31,000	1.000	2.500	2.750	2.000	.313
6	39,000	1.000	1.500	1.750	1.500	.313
5	39,000	1.000	2.000	2.250	1.750	.313
10	39,000	1.000	2.000	2.250	2.000	.375
17	39,000	1.000	1.500	1.750	1.500	.313
16	124,000	1.000	2.500	2.750	1.500	.375
143	78,000	1.000	2.000	2.250	1.500	.188
141	78,000	1.000	2.000	2.250	1.750	.187
142	78,000	1.000	2.000	2.250	1.750	.174
140	78,000	1.000	1.500	1.750	1.500	.188
138	78,000	1.000	2.000	2.250	1.500	.139
139	78,000	1.000	2.000	2.250	1.500	.203
131	31,000	1.000	2.000	2.250	2.250	.432
132	39,000	1.000	2.000	2.250	1.625	.196
133	39,000	1.000	1.500	1.750	1.500	.191
127	31,000	1.000	3.500	3.750	3.750	1.750
126	237,000	1.000	3.500	3.750	3.500	1.750
134	79,000	1.000	3.000	3.250	3.000	.688
135	316,000	1.000	4.000	4.250	4.000	2.000
125	79,000	1.000	2.500	2.750	2.500	1.250
101	40,000	1.000	2.000	3.000	3.000	1.000
100	97,000	1.000	3.000	3.250	4.000	2.250
119	158,000	1.000	3.500	3.750	3.750	1.750
120	79,000	1.000	3.000	3.250	3.500	1.460
123	210,000	1.000	3.500	3.500	3.000	1.500
122	79,000	1.000	2.500	2.750	3.250	.906
121	79,000	1.000	2.750	3.000	3.000	.800
120	79,000	1.000	3.250	3.250	3.750	1.250
113	158,000	1.000	4.500	4.750	4.000	2.250
112	316,000	1.000	3.000	3.500	2.750	1.000
129	79,000	1.000	3.250	3.500	2.500	.600
114	119,000	1.000	3.500	3.750	1.000	1.200
115	237,000	1.000	2.750	3.000	2.750	.700
116	118,000	1.000	4.000	3.250	4.250	2.000
117	118,000	1.000	3.000	3.000	3.250	1.000
118	118,000	1.000	3.500	2.750	3.750	1.200
119	118,000	1.000	2.500	3.500	3.000	1.000
131	316,000	1.000	3.000	3.500	3.500	1.250
134	316,000	1.000	3.750	4.500	3.750	1.500
95	145,500	2.000	6.000	6.000	6.000	6.000
83	145,500	2.000	6.000	6.750	6.000	7.250
82	145,500	2.000	5.500	5.250	6.000	6.000
79	145,500	2.000	8.000	5.000	7.000	11.000
86	291,000	2.000	6.000	7.000	6.500	9.500
85	291,000	2.000	5.000	5.000	6.000	8.250
80	194,000	2.000	6.000	5.000	6.000	8.500
81	194,000	2.000	6.000	6.750	6.000	6.750
78	194,000	2.000	5.500	6.000	6.000	6.500
76	194,000	2.000	7.000	4.000	6.500	6.500
75	194,000	2.000	7.500	6.500	7.000	8.000
74	194,000	2.000	7.000	6.000	7.000	8.500
87	242,000	2.000	5.000	6.500	6.000	6.250
77	194,000	2.000	6.000	6.000	6.000	6.500
88	238,000	2.000	6.000	5.000	5.375	4.500
89	238,000	2.000	5.500	6.500	6.500	8.500

WEDGE TIP ANALYSIS- 2 IN. 90 DEGREE EDGE

ROW NO.	LOADING LB/IN.	A IN.	B IN.	C IN.	D IN.	DOCK RESISTANCE LB
91	234.000	2.000	7.000	8.000	7.000	10.000
92	234.000	2.000	7.000	7.500	7.000	10.000
93	234.000	2.000	7.000	7.500	7.000	9.000
94	234.000	2.000	8.000	6.000	8.000	10.000
73	234.000	2.000	7.000	7.000	7.000	7.000
103	219.500	2.000	6.000	4.500	6.500	6.750
105	340.000	2.000	8.000	5.000	6.750	9.000
106	315.500	2.000	6.500	6.500	6.500	9.000
104	315.500	2.000	6.500	5.500	6.500	8.000
96	582.000	2.000	9.000	9.000	8.000	10.000
97	582.000	2.000	9.000	9.000	6.500	10.000
98	582.000	2.000	9.000	9.000	6.750	14.000
99	582.000	2.000	9.000	9.000	7.500	14.000
100	582.000	2.000	9.000	9.000	7.250	11.750
101	582.000	2.000	9.000	9.000	8.500	14.750

POINTED INDENTOR TESTS- STATISTICAL ANALYSIS

	A	B1	B2	B	H	ROCK WEIGHT	ROCK VOLUME
GHTED AVERAGE	.50	1.795	1.984	1.[illegible]15	1.[illegible]6	.154	1.667
GHTED MEAN	.50	1.[illegible]16	1.[illegible]25	1.[illegible]99	1.866	.162	
NDARD DEVIATION	.50	.075	.090	.[illegible]97	.[illegible]1	.014	
GHTED AVERAGE	1.00	2.363	2.[illegible]32	2.[illegible]1[illegible]	2.[illegible]7	.504	6.094
GHTED MEAN	1.00	2.445	2.[illegible]35	2.[illegible]16	[illegible].[illegible]16	.659	
NDARD DEVIATION	1.00	.166	.158	.162	.[illegible]1	.077	
GHTED AVERAGE	2.00	4.381	4.385	4.[illegible]3[illegible]	5.[illegible]27	5.[illegible]43	36.456
GHTED MEAN	2.00	4.617	4.791	4.[illegible]35	5.[illegible]12	4.[illegible]36	
NDARD DEVIATION	2.00	.325	.431	.3[illegible]2	.[illegible]26	.451	

WEDGE TIP ANALYSIS- 2 1%, 90 DEGREE WEDGE

	A	B1	B2	B	H	ROCK WEIGHT	ROCK VOLUME
GHTED AVERAGE	.50	2.125	2.124	1.125	1.633	.213	2.224
GHTED MEAN	.50	2.162	2.167	1.194	1.[illegible]55	.[illegible]02	
NDARD DEVIATION	.50	.094	.098	.[illegible]96	.075	.024	
GHTED AVERAGE	1.00	3.199	3.291	2.246	3.[illegible]5[illegible]	1.[illegible]92	12.439
GHTED MEAN	1.00	3.[illegible]43	3.328	2.[illegible]85	3.[illegible]27	1.[illegible]74	
NDARD DEVIATION	1.00	.095	.061	.[illegible]89	.[illegible]4[illegible]	.09[illegible]	
GHTED AVERAGE	2.00	6.905	6.612	5.759	6.[illegible]02	8.[illegible]09	91.917
GHTED MEAN	2.00	7.[illegible]13	6.784	5.[illegible]62	6.704	9.[illegible]05	
NDARD DEVIATION	2.00	.209	.252	.233	.075	.415	

APPENDIX C

NON-ISOTROPIC BEHAVIOR OF LARAMIE GRANITE

We have ignored in the earlier analysis any anisotropy present in the rock. The analytical problems when anisotropy is included become complicated, and on the experimental side, the number of tests required to obtain statistically meaningful data becomes astronomical.

A simplifying assumption can be introduced in that the elastic properties (E and ν) can be assumed to be isotropic. This assumption, although it cannot be defended too vigorously, lets one use the available solution to yield some estimate of volume removed and critical energies required to initiate the fracture. Let us further assume that the elastic axes are parallel to the edges of the block. Finally, in view of the layered nature of granite* we can assume strength properties in directions 1 and 2 (see Figure C-1) to be the same. Thus,

$$\sigma_{t_1} = \sigma_{t_2} > \sigma_{t_3}$$

where subscripts 1, 2, and 3 represent the directions shown in Figure

A total of six edge fracture combinations are possible as shown in Table C-1. Of these six (refer to Fig. C-1), numbers 1 and 3 (now labeled Mode M-1) are identical, numbers 2 and 4 (labeled M-2) are identical, and numbers 5 and 6 (M-3) are identical.

Now, as before, when $\sigma_{x_{max}} = \sigma_{t_i}$, the fracture initiates. Thus, in general there will be three different critical energies but since σ_t is the same in two of the directions, two of the energies will be identical. Let us use subscript "i" to designate these energy levels as follows:

$$E_{cr_i} = \left[\frac{\sigma_{t_i}\, a^2}{2kc} \right]^{\frac{1}{n}}$$

* Wagner & Brown. "Layered Igneous Rocks." Freeman & Co. (San Francisco, 1967).

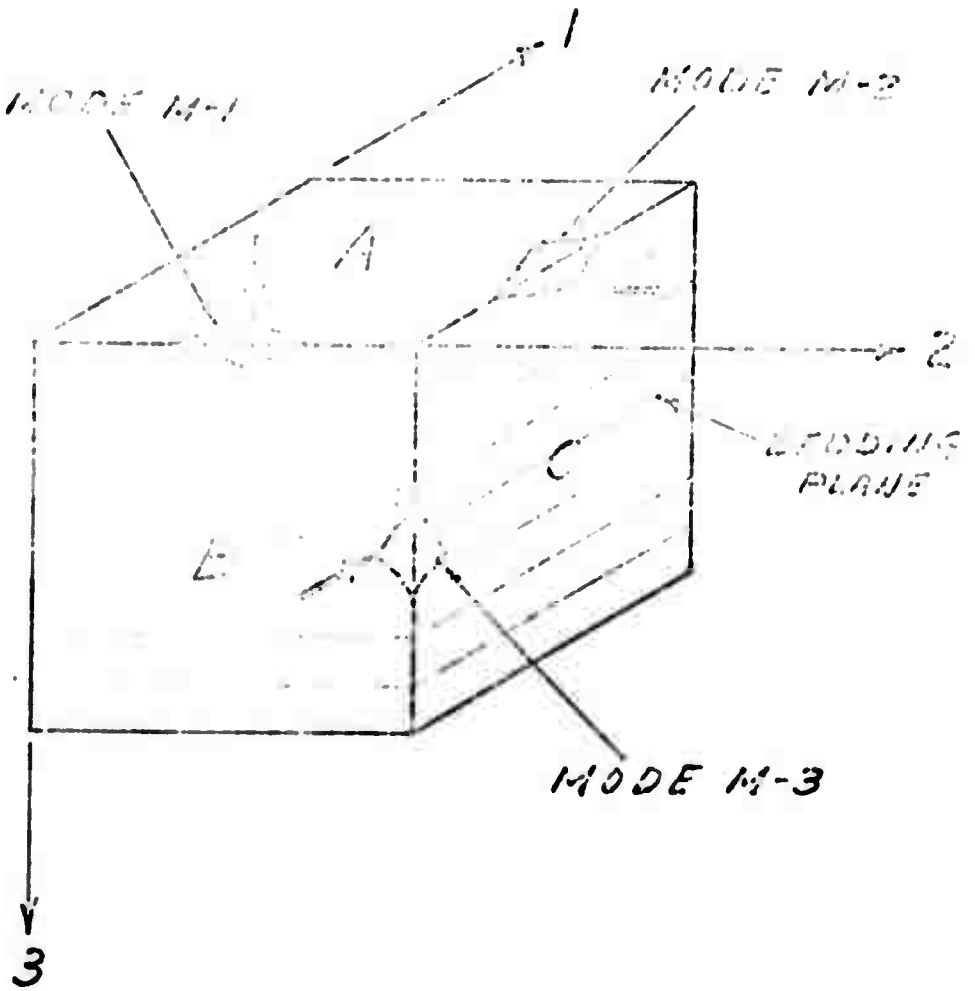

Figure C-1: Face, Edge and Fracture Mode Designation

	tool normal / fracturing to surface / into surface	Mode
1	A-B	M-1
2	B-A	M-2
3	A-C	M-1
4	C-A	M-2
5	B-C	M-3
6	C-B	M-3

TABLE C-I
FRACTURE MODES

Example: A-B means tool is normal to the face A, and the breakout is to the face B as illustrated by M-1 in Figure C-1.

C-a

The fracture size was determined in the isotropic case by b and h. Now three combinations of b and h are possible.

$$h_i \; ; \; b_i = b, \; t \quad \text{for Mode M-i in Table C-1.}$$

Also, the volumes are given by

$$V_i = \frac{\lambda}{3} \, a \, b_i \, h_i$$

i = 1 to 3 according to Mode number M-1 to M-3. Plate C-1 clearly shows the three distinct volumes consigned to the three modes. Thus, three different volumes should also be expected. In spite of the test to test variation in rock, such distinction in the volumes was indeed observed.

When fracture occurs in Modes M-1 and M-3, one uses $\sigma_t = \sigma_{t_1}$ and for M-2, use $\sigma_t = \sigma_{t_3}$. Thus, the fracture energy for Mode 2 is larger than that for Modes M-1 and M-3. Since b and h depend on peak loads and tensile strengths, three distinct fracture volumes will, in general, be observed. Plate C.-1 shows typical fractures.

In practice the alignment between geometric and elastic axes is difficult to achieve, although the mining and cutting operations tend to produce some alignment. The effects of mis-alignment can be reduced somewhat by selective averaging technique. On Figure C-2 we show the experimental data from Table 3, Appendix A. It is estimated that in two of the directions the critical energy is of the order of 95 ft lb while in the third direction it may be as high as 238 ft lb. In breaking out at a single blow at the lower energy the rock volume is smaller than that when breaking out at higher blow energy. Thus in one of the directions the critical energy is higher and the breakout volume is larger while in the other two directions critical energy is smaller and there are two different volumes that breakout at this level. The available data seems to be consistent with the above concepts. However, the total number of tests is too small to allow any positive (or negative) conclusions.

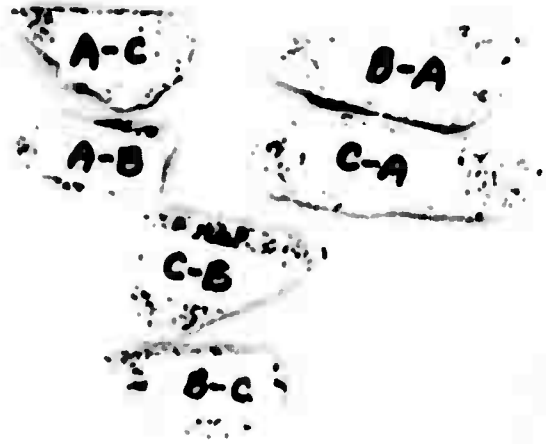

Plate C-1: Typical three-mode fractures

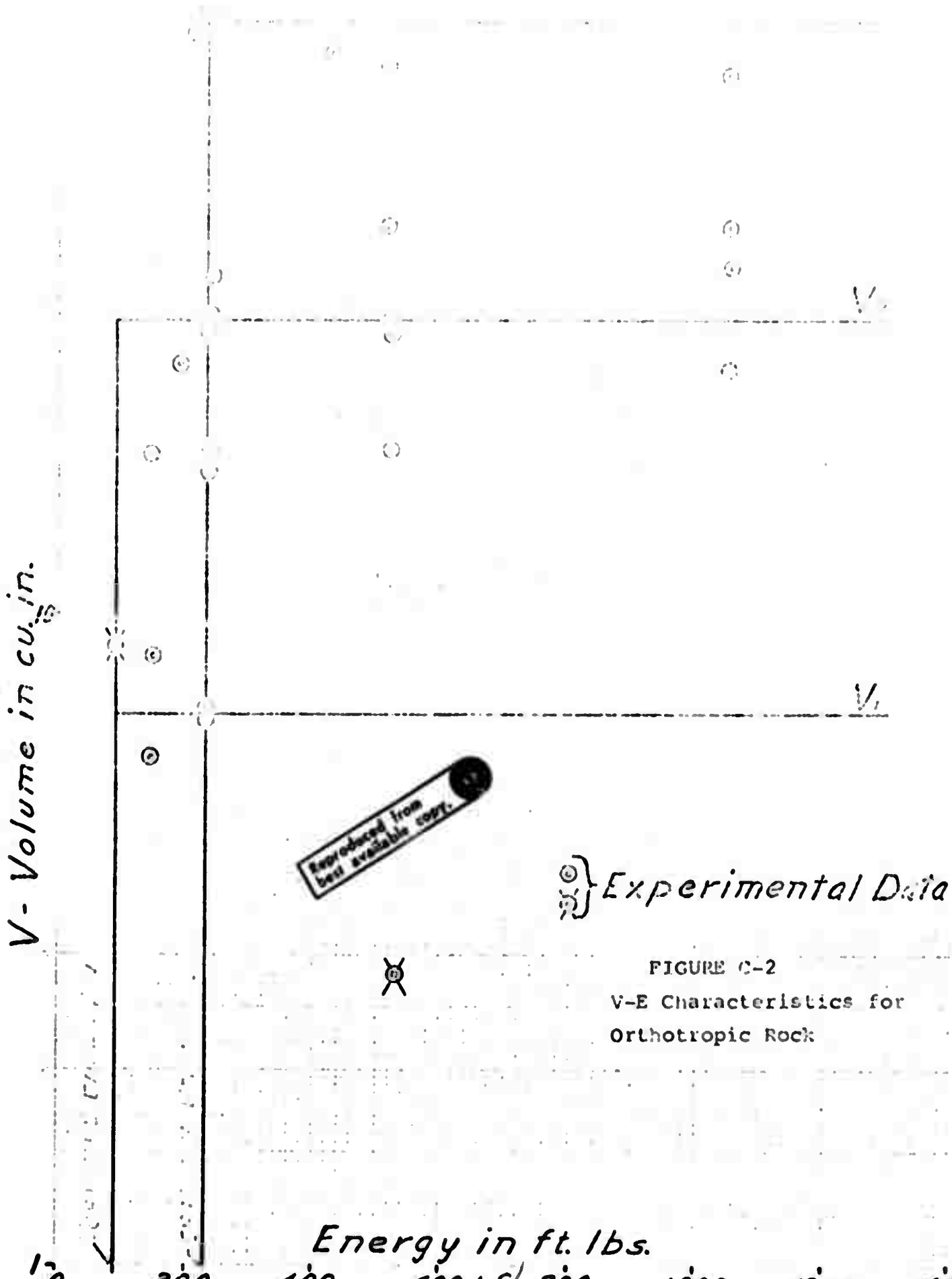

FIGURE C-2
V-E Characteristics for
Orthotropic Rock